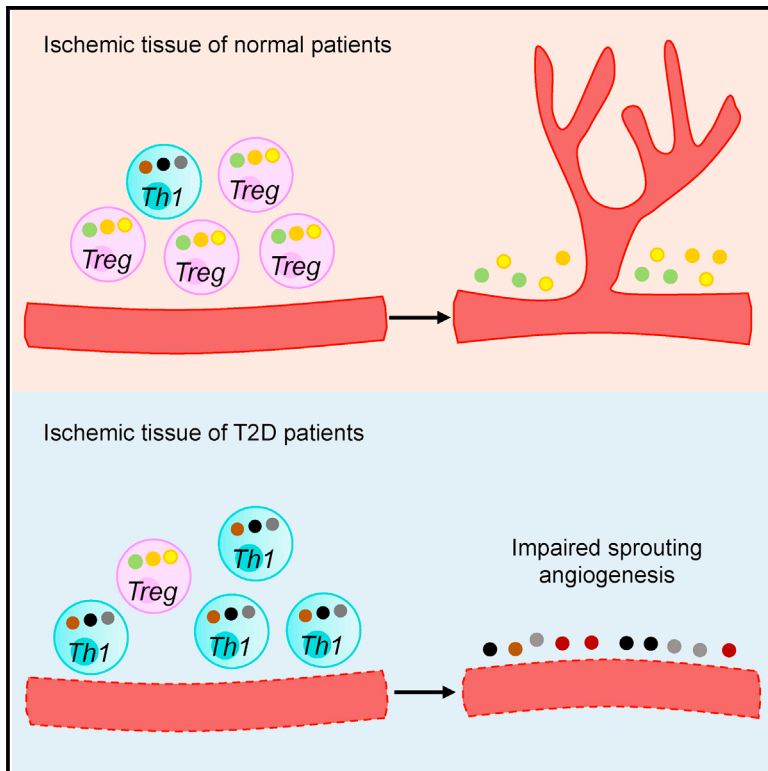


Regulatory T Cells Promote Apelin-Mediated Sprouting Angiogenesis in Type 2 Diabetes

Graphical Abstract



Authors

Oscar M. Leung, Jiatao Li, Xisheng Li, ..., James Lau, Bin Zhou, Kathy O. Lui

Correspondence

kathyolui@cuhk.edu.hk

In Brief

There are significantly more CD4⁺ Th1 cells but fewer regulatory T cells (Tregs) in ischemic tissues from T2D patients than from normoglycemic patients with peripheral artery disease. Leung et al. show that Th1 cells impair vascular regeneration in T2D individuals in a paracrine manner, while Tregs potentiate regeneration.

Highlights

- More CD4⁺ T cells and fewer Tregs are found in T2D patients with PAD
- CD4⁺ Th1 cells inhibit *de novo* sprouting angiogenesis in T2D
- IFN- γ and TNF- α inhibit endothelial cell function
- IL-10 and amphiregulin promote endothelial cell proliferation and function



Regulatory T Cells Promote Apelin-Mediated Sprouting Angiogenesis in Type 2 Diabetes

Oscar M. Leung,^{1,2,10} Jiatao Li,^{1,2,10} Xisheng Li,^{1,10} Vicken W. Chan,¹ Kevin Y. Yang,¹ Manching Ku,^{3,4} Lu Ji,^{1,2} Hao Sun,^{1,2} Herman Waldmann,⁵ Xiao Yu Tian,^{6,7} Yu Huang,^{2,6,7} James Lau,⁸ Bin Zhou,⁹ and Kathy O. Lui^{1,2,11,*}

¹Department of Chemical Pathology, Prince of Wales Hospital, The Chinese University of Hong Kong, Hong Kong SAR, China

²Li Ka Shing Institute of Health Sciences, Prince of Wales Hospital, The Chinese University of Hong Kong, Hong Kong SAR, China

³Next Generation Sequencing Core, Salk Institute for Biological Studies, La Jolla, CA, USA

⁴Department of Paediatrics and Adolescent Medicine, Division of Paediatric Hematology and Oncology, Medical Center, Faculty of Medicine, University of Freiburg, Freiburg, Germany

⁵Sir William Dunn School of Pathology, University of Oxford, Oxford, UK

⁶School of Biomedical Sciences, The Chinese University of Hong Kong, Hong Kong SAR, China

⁷Institute of Vascular Medicine, The Chinese University of Hong Kong, Hong Kong SAR, China

⁸Department of Surgery, Prince of Wales Hospital, The Chinese University of Hong Kong, Hong Kong SAR, China

⁹The State Key Laboratory of Cell Biology, CAS Center for Excellence in Molecular Cell Science, Shanghai Institute of Biochemistry and Cell Biology, Chinese Academy of Sciences, University of Chinese Academy of Sciences, Shanghai, China

¹⁰These authors contributed equally

¹¹Lead Contact

*Correspondence: kathyolui@cuhk.edu.hk

<https://doi.org/10.1016/j.celrep.2018.07.019>

SUMMARY

The role of CD4⁺ T cells in the ischemic tissues of T2D patients remains unclear. Here, we report that T2D patients' vascular density was negatively correlated with the number of infiltrating CD4⁺ T cells after ischemic injury. Th1 was the predominant subset, and Th1-derived IFN- γ and TNF- α directly impaired human angiogenesis. We then blocked CD4⁺ T cell infiltration into the ischemic tissues of both *Lepr^{db/db}* and diet-induced obese T2D mice. Genome-wide RNA sequencing shows an increased proliferative and angiogenic capability of diabetic ECs in ischemic tissues. Moreover, wire myography shows enhanced EC function and laser Doppler imaging reveals improved post-ischemic blood reperfusion. Mechanistically, functional revascularization after CD4 coreceptor blockade was mediated by Tregs. Genetic lineage tracing via *Cdh5-CreER* and *Apln-CreER* and coculture assays further illustrate that Tregs increased vascular density and induced *de novo* sprouting angiogenesis in a paracrine manner. Taken together, our results reveal that Th1 impaired while Tregs promoted functional post-ischemic revascularization in obesity and diabetes.

INTRODUCTION

Peripheral artery disease (PAD) often has been diagnosed in the aging population; however, there is an increasing incidence of PAD in the younger population as a result of the global diabetes

epidemic (Steinberger et al., 2003). Type 2 diabetes (T2D) in particular promotes atherosclerosis and endothelial dysfunction with progression to critical limb ischemia (CLI); 30% of T2D patients require amputations, with a severely compromised survival rate (Howard et al., 2015). To date, there are few if any effective strategies to slow the progression of CLI. Although numerous mediators, including proangiogenic factors, transcription factors, and signaling molecules, have been implicated in promoting functional revascularization in normoglycemic animal models after physically induced ischemia, clinical trials targeting these pathways for medical revascularization in diabetic patients have been largely disappointing (Raval and Losordo, 2013). Therefore, more studies are needed to understand the pathogenesis between normoglycemic and diabetic PAD and to unravel specific treatments targeting diabetic PAD.

It has been reported that new blood vessels are regenerated via sprouting angiogenesis after ischemic injury in normoglycemic mice. Accumulating evidence reveals that infiltrating T cells in the ischemic sites facilitate that revascularization. Athymic nude mice that lack T cells exhibit a reduced capability for post-ischemic revascularization (Couffignal et al., 1999). Revascularization is also impaired in CD4-deficient mice after ischemic injury (Stabile et al., 2003). Moreover, it has been demonstrated that interleukin (IL)-17 deficiency leads to significantly reduced post-ischemic blood perfusion (Hata et al., 2011), suggesting that IL-17-producing CD4⁺ T_H17 cells are required for vascular regeneration. Nevertheless, obese adipose tissues of both rodents and humans show hallmarks of chronic inflammation with recruitment of different T cell subsets (Feuerer et al., 2009; Nishimura et al., 2009; Winer et al., 2009; McLaughlin et al., 2014) known to play an instrumental role in the development of insulin resistance (McLaughlin et al., 2014). Whether these infiltrating CD4⁺ T cells regulate vascular regeneration in diabetic PAD remains unknown.



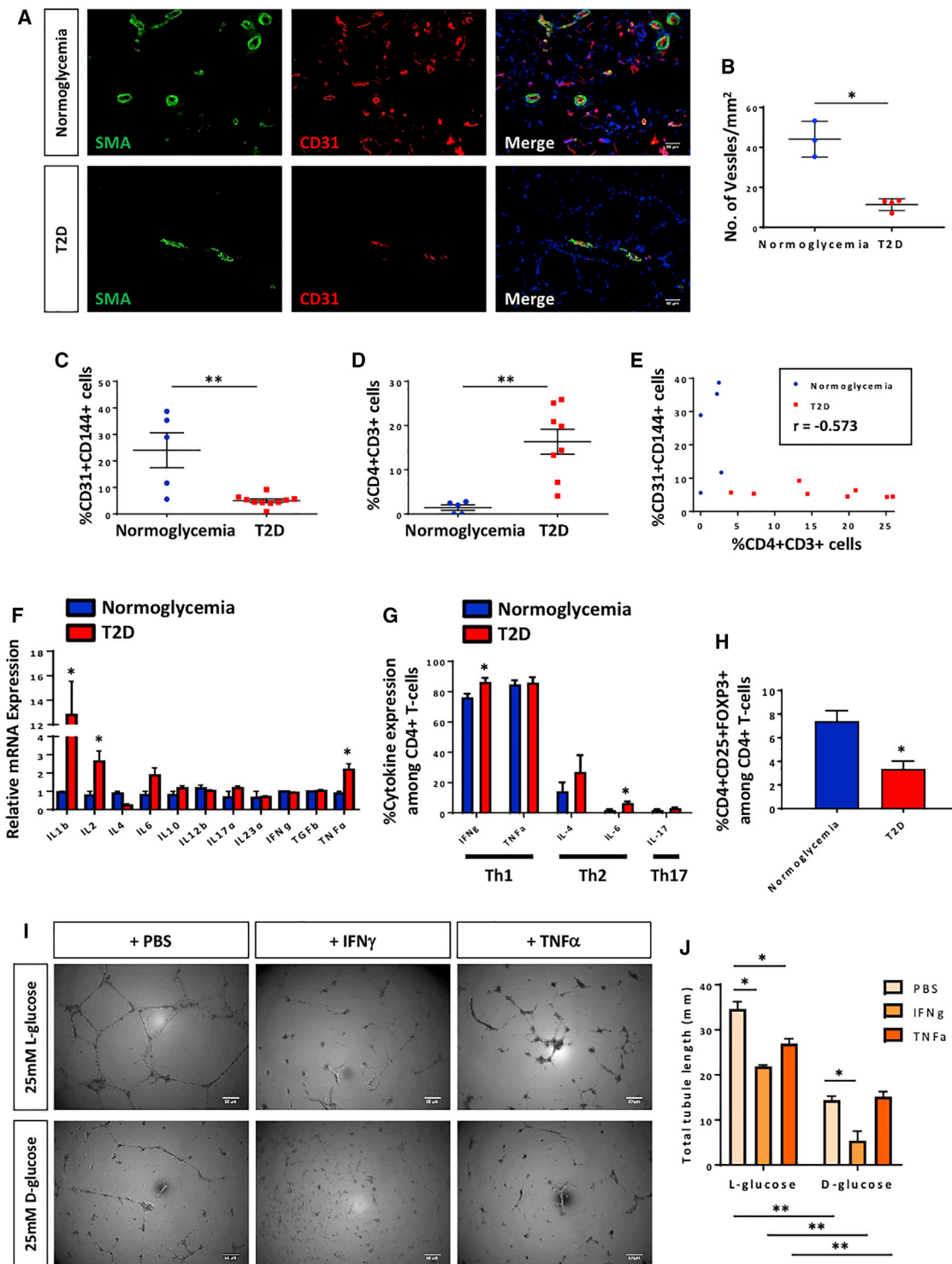


Figure 1. CD4⁺ Th1 Subset Impairs Vascular Growth and Function in T2D

(A and B) (A) Immunostaining on frozen sections and (B) quantification for SMA⁺ (green) and CD31⁺ (red) cells with nuclear DAPI counterstain (blue) showing a significantly reduced number of blood vessels per unit area in ischemic muscles of T2D (n = 4) than normoglycemic (n = 3) patients with PAD after below-the-knee amputation. Scale bars: 40 μ m.

(C and D) Flow cytometric quantification of (C) %CD31⁺CD144⁺ or (D) %CD4⁺CD3⁺ cells in the ischemic muscles of normoglycemic (n = 5) or T2D (n = 8) patients.

(E) Scatterplots showing a negative correlation between EC density and CD4⁺ T cell infiltration into the ischemic muscles of normoglycemic and T2D patients.

(F) qRT-PCR of purified CD31⁺CD144⁺ ECs from (C). Gene expression levels in T2D were compared to normoglycemic patients.

(legend continued on next page)

CD4⁺ regulatory T cells (Tregs) are potent suppressors of the immune system. Emerging evidence demonstrates that they accumulate in injured tissues and promote wound healing and regeneration of multiple organ systems, including heart muscle (Weirather et al., 2014), skeletal muscle (Burzyn et al., 2013), skin (Ali et al., 2017), and central nervous (Dombrowski et al., 2017). Nevertheless, it remains unclear whether they are involved in the regeneration of the peripheral vascular system. Here, we investigate whether infiltrating CD4⁺ T cells in ischemic tissues regulate vascular regeneration in T2D by blocking their ability to respond to self-antigens expressed after injury via coreceptor blockade with a non-lytic anti-CD4 monoclonal antibody (mAb) previously used to promote antigen-specific tolerance with the induction of Tregs in the transplantation setting (Lui et al., 2010, 2014). We demonstrate that CD4 coreceptor blockade led to reduced vascular inflammation, promoted endothelial cell (EC) proliferation, and enhanced vascular function via apelin (Apln)-mediated sprouting angiogenesis. Such improvements were facilitated by Tregs. Dissimilar from normoglycemia, our results reveal that CD4⁺ effector T cells impaired while Tregs promoted functional post-ischemic revascularization in T2D.

RESULTS

CD4⁺ Th1 Subset Impairs Vascular Growth and Function in Hyperglycemia

We asked whether there was any correlation between vascular density and tissue infiltration of CD4⁺ T cells in T2D patients. We collected the gastrocnemius muscles and nearby arteries of amputated limbs from both normoglycemic (*n* = 8) and T2D (*n* = 12) patients with PAD (Table S1). We performed co-staining for specific markers of smooth muscle cells: smooth muscle actin (SMA) and ECs: CD31 (Figure 1A). Our results showed that T2D patients had significantly reduced SMA⁺CD31⁺ blood vessels compared to normoglycemic patients (Figure 1B). We confirmed EC density by flow cytometry (Figure S1A) and found that there were significantly reduced %CD31⁺CD144⁺ vessel ECs in T2D than in normoglycemic patients (Figure 1C). Alternatively, we demonstrated that there were significantly increased %CD4⁺CD3⁺ T cells in T2D than in normoglycemic patients (Figures 1D and S1B). Statistical analysis confirmed the negative correlation between vascular density and tissue infiltration of CD4⁺ T cells in normoglycemic and T2D patients (Figure 1E; Pearson's correlation coefficient *r* = −0.573). Our qPCR data also suggested that T2D ECs could facilitate T cell activation and proliferation because there were significantly upregulated genes, including *Il1b*, *Il2*, and *Tnfa*, expressed by the purified CD31⁺CD144⁺ vessel ECs of T2D than of normoglycemic patients (Figure 1F).

To investigate which CD4⁺ T cell subset impaired angiogenesis, we performed intracellular cytokine staining, including Th1-specific interferon- γ (IFN- γ) and tumor necrosis factor- α

(TNF- α), Th2-specific IL-4 and IL-6, and Th17-specific IL-17 by flow cytometry (Figure S2A). We revealed that Th1 cells were predominantly present in the ischemic tissues of patients because approximately 80% of CD4⁺ T cells expressed IFN- γ and TNF- α , and the expression levels of IFN- γ and IL-6 were significantly upregulated in T2D than in normoglycemic patients (Figure 1G). Moreover, our flow cytometric analysis showed significantly reduced %CD4⁺CD25⁺FOXP3⁺ Tregs among total CD4⁺ T cells in ischemic tissues of T2D than of normoglycemic patients (Figures 1H and S2B). To ask how Th1 cells contributed to reduced vascular density in T2D patients, we cultured mature human embryonic stem cell (hESC)-ECs in 25 mM L- or D-glucose with solvent control (PBS) or Th1 cytokines, respectively (Figure 1I). L-glucose served as an osmotic control for D-glucose and did not affect the *in vitro* angiogenesis (tube formation) of hESC-ECs. More important, D-glucose significantly reduced the total tubule length of hESC-ECs compared to L-glucose (Figure 1J), suggesting that the high glucose level directly impaired angiogenesis. Moreover, IFN- γ and TNF- α significantly reduced the total tubule length of hESC-ECs in L-glucose compared to PBS, and the same concentration significantly impaired *in vitro* angiogenesis in D- than in L-glucose. Taken together, Th1 cells impaired angiogenesis in a paracrine manner.

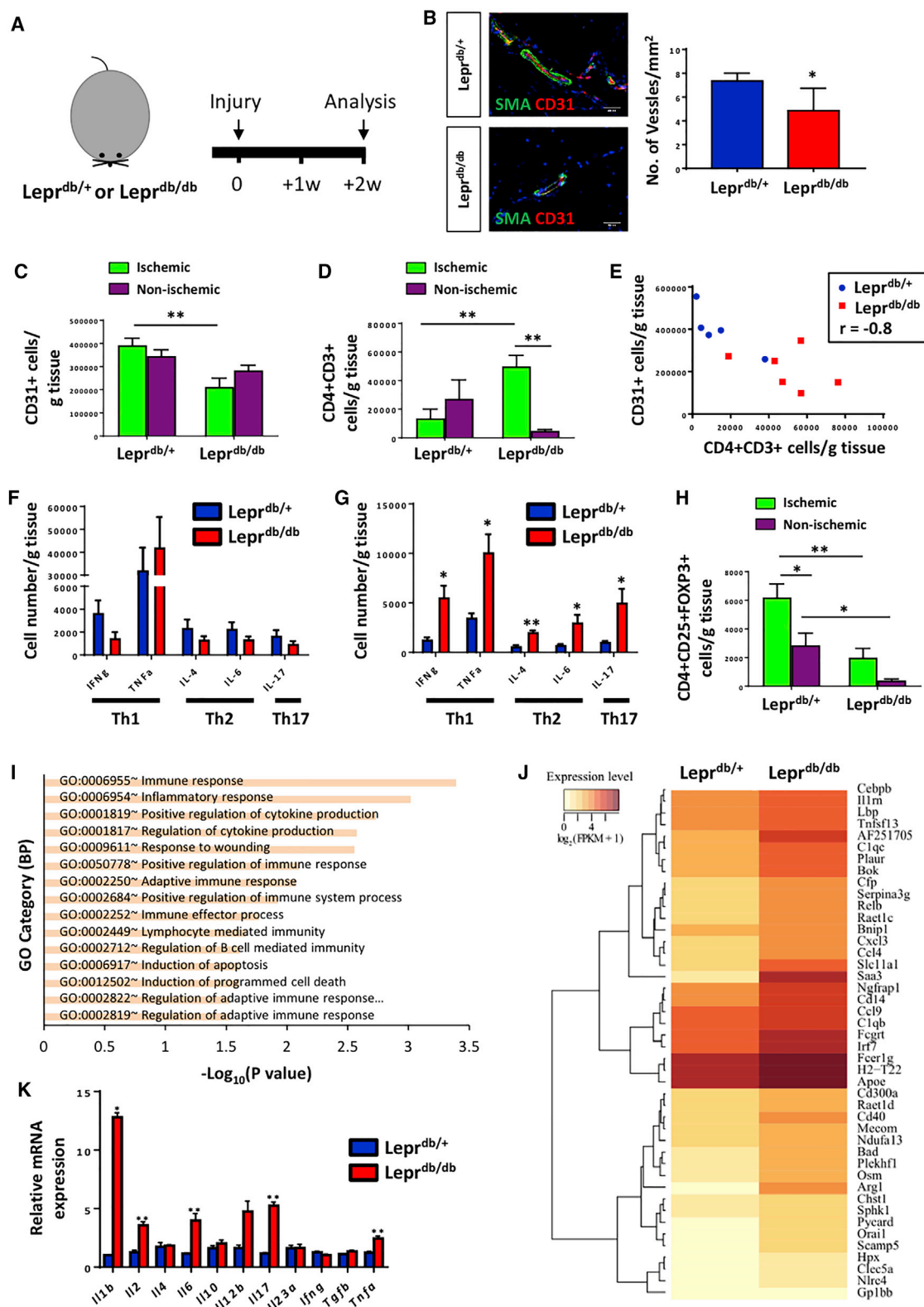
Diabetic Endothelial Cells Are Pro-inflammatory

Previous studies revealed that CD4⁺ T cells are required for post-ischemic revascularization in normoglycemic mice (Stabile et al., 2003; van Weel et al., 2007; Hata et al., 2011); yet, whether they facilitate that revascularization in T2D remains unknown. To address this question, we generated a severe hindlimb ischemia model in *Lepr^{db/+}* and *Lepr^{db/db}* mice that recapitulated PAD in normoglycemic and T2D patients, respectively. To examine the endogenous capability of T2D mice for vascular regeneration, we compared vessel density, EC density, and post-ischemic reperfusion of *Lepr^{db/+}* and *Lepr^{db/db}* mice by immunostaining, flow cytometry, and laser Doppler imaging, respectively (Figure 2A). Our results showed a significantly reduced number of SMA⁺CD31⁺ blood vessels (Figure 2B) and CD45⁺CD31⁺ ECs (Figures 2C, S3A, and S3B) in the ischemic muscles of *Lepr^{db/db}* than in *Lepr^{db/+}*. *Lepr^{db/db}* also exhibited significantly impaired post-ischemic reperfusion compared to *Lepr^{db/+}* (Figure S4). In addition, we found that the number of CD4⁺CD3⁺ T cells was significantly increased in the ischemic muscles of *Lepr^{db/db}* compared to its non-ischemic muscles or to those of *Lepr^{db/+}* (Figures 2D, S3A, and S3C). The number of CD4⁺ T cells was negatively correlated to the number of ECs in the ischemic muscles of *Lepr^{db/+}* and *Lepr^{db/db}* (*r* = −0.8; Figure 2E), which is in line with the human data (Figure 1E). Moreover, we demonstrated that various CD4⁺ T cell subsets did not differ in quantity in the non-ischemic muscles of *Lepr^{db/+}* and *Lepr^{db/db}* (Figure 2F); however, the numbers of Th1, Th2, and Th17 cells were significantly increased in the ischemic tissues of *Lepr^{db/db}* than in

(G and H) Flow cytometric quantification of (G) various CD4⁺ T cell subsets or (H) CD4⁺CD25⁺FOXP3⁺ Treg in the ischemic muscles of normoglycemic (*n* = 3) and T2D (*n* = 4) patients, respectively.

(I and J) (I) *In vitro* tube formation assay (scale bars: 50 μ m) and (J) quantification of the total tubule length of hESC-ECs cultured under normoglycemic (25 mM L-glucose) or hyperglycemic (25 mM D-glucose) conditions with IFN- γ or TNF- α , respectively.

All data (B–D, F–H, and J) are presented as means \pm SEMs. **p* < 0.05, ***p* < 0.01.



(legend on next page)

Lepr^{db/+} (Figure 2G). We also found that the number of CD4⁺CD25⁺FOXP3⁺ Tregs was significantly increased in Lepr^{db/+} post-ischemia (Figure 2H). However, this increase was not significant in Lepr^{db/db} and the number of CD4⁺CD25⁺FOXP3⁺ Tregs in the ischemic and non-ischemic muscles of Lepr^{db/db} was significantly less than that of Lepr^{db/+}. Taken together, our results from the analogous mouse model were consistent with the human data that showed significantly more CD4⁺ T cells—predominantly, the Th1 subset and reduced Tregs in the ischemic muscles of T2D than in control mice.

To delineate the phenotypic difference in the ECs of Lepr^{db/+} and Lepr^{db/db}, we purified CD45⁺CD31⁺ ECs from ischemic muscles by flow cytometry and performed genome-wide transcriptomic profiling by RNA sequencing (RNA-seq). A total of 13,555 protein-coding genes were identified, 1,028 of which were differentially expressed in the ECs of Lepr^{db/db} than in Lepr^{db/+}. These differentially expressed genes were then analyzed with functional annotations by Gene Ontology (GO) enrichment analyses to identify genes and/or gene sets that are involved in biological processes. Our results showed that the top 15 significantly upregulated pathways in diabetic ECs were associated with innate and immune responses (Figure 2I; Table S2). The differentially expressed genes of these pathways were also demonstrated by heatmap (Figure 2J). We validated some of these data by qPCR, with a focus on cytokine production. We found significantly upregulated gene expression of the pro-inflammatory cytokines, including *Il1b*, *Il2*, *Il6*, *Il17*, and *Tnfa*, in ECs of Lepr^{db/db} than in Lepr^{db/+} (Figure 2K). Our results were consistent with the human data that T2D ECs were pro-inflammatory (Figure 1F).

CD4 Coreceptor Blockade Reduces Vascular Inflammation and Promotes Vascular Regeneration in Lepr^{db/db}

To elucidate the role of CD4⁺ T cells in therapeutic angiogenesis in T2D, we blocked their activation, proliferation, and/or infiltration using a non-lytic anti-CD4 mAb (clone YTS177) as previously described (Lui et al., 2010, 2014) and examined revascularization at 4 weeks after ischemia (Figure 3A). While anti-CD4 mAb did not affect recipients' blood glucose level or body weight, there were increased EC density (Figures 3B, S5A, and S5B) and reduced infiltration of CD4⁺CD3⁺ T cells (Figures 3C, S5A, and S5C), with a significant negative correlation coefficient ($r = -0.7$; Figure 3D) in the ischemic muscles of YTS177-treated

than in isotype control immunoglobulin G2a (IgG2a)-treated Lepr^{db/db} mice. It is important to note that YTS177 induces the internalization of CD4 molecules, so we performed both surface and intracellular staining for CD4. Although the number of CD4⁺ T cells were significantly reduced in both ischemic and non-ischemic muscles after YTS177 treatment, only the EC density of ischemic muscles was altered, suggesting an antigen-specific effect for YTS177 in response to neoantigen after injury. We also examined capillary density by immunostaining for CD31, as previously described (Kikuchi et al., 2014), and observed significantly more CD31⁺ capillaries in the ischemic muscles of YTS177-treated than of the IgG2a-treated group (Figure S6A). In line with the flow cytometric data (Figure 3B), our findings revealed that the beneficial effect of YTS177 on revascularization was localized to ischemic tissues because there was no difference in the capillary density of non-ischemic tissues between YTS177-treated and IgG2a-treated groups.

To delineate the phenotypic difference in diabetic ECs after CD4 coreceptor blockade, we purified CD45⁺CD31⁺ ECs from the ischemic muscles of IgG2a-treated or YTS177-treated mice by flow cytometry. We performed quality control of sorted ECs by qPCR and confirmed that they significantly upregulated EC-specific genes such as *Pecam-1* (CD31), *Cdh5* (CD144), and *Flk-1* 20- to 200-fold and did not express pericyte and/or smooth muscle cell-specific genes such as *Pdgfr-β* and *Smmhc* (Figure S6B). We then performed RNA-seq and found a total of 1,107 protein-coding genes differentially expressed in diabetic ECs treated with YTS177 rather than IgG2a. Our results showed that the top 10 pathways in terms of biological processes that were significantly upregulated in YTS177-treated ECs were associated with cell proliferation (Figure 3E; Table S3). The differentially expressed genes of these pathways were demonstrated by heatmap (Figure 3F). To validate our RNA-seq data, we performed immunostaining and found significantly increased %Ki67⁺CD31⁺ cells among total CD31⁺ ECs in the ischemic muscles of the YTS177-treated group than in the IgG2a-treated group (Figure 3G), indicating increased EC proliferation after YTS177 treatment (Figure 3H). Moreover, we found a significantly increased number of SMA⁺CD31⁺ blood vessels in the ischemic muscles of the YTS177-treated group than in the IgG2a-treated group (Figures 3G and 3I).

Furthermore, to confirm increased post-ischemic angiogenesis in YTS177-treated mice, we performed qPCR to score for gene expression of angiogenic factors. We found significantly

Figure 2. Reduced Vascular Density and Increased Vascular Inflammation in the Ischemic Tissues of Lepr^{db/db} Mice

- (A) Schematic diagram showing the experimental design (n = 20/group).
 (B) Immunostaining on frozen sections and quantification for SMA⁺ (green) and CD31⁺ (red) cells with nuclear DAPI counterstain (blue) showing a significantly reduced number of blood vessels per unit area in the ischemic muscles of Lepr^{db/db} than Lepr^{db/+} mice. Scale bars: 40 μm.
 (C and D) Flow cytometric quantification showing absolute number of (C) CD31⁺ or (D) CD4⁺CD3⁺ cells/g tissue in the ischemic and non-ischemic muscles after being gated on CD45⁺ or CD45⁺ cells, respectively.
 (E) Scatterplots showing a negative correlation between EC density and CD4⁺ T cell infiltration into the ischemic muscles of Lepr^{db/+} and Lepr^{db/db}.
 (F–H) Flow cytometric quantification of various CD4⁺ T cell subsets in (F) non-ischemic or (G) ischemic muscles or (H) CD4⁺CD25⁺FOXP3⁺ Treg in the ischemic muscles of Lepr^{db/+} and Lepr^{db/db}.
 (I and J) Genome-wide RNA-seq results showing (I) the top 15 most significant biological processes as determined by upregulated genes expressed by CD45⁺CD31⁺ ECs purified from the ischemic muscles of Lepr^{db/db} compared to Lepr^{db/+} mice, and (J) differentially expressed genes on heatmap as determined by GO functional clustering.
 (K) Quantitative RT-PCR of CD45⁺CD31⁺ ECs purified from (C). Gene expression levels in Lepr^{db/db} were compared to Lepr^{db/+} mice.
 All data (B–D, F–H, and K) are presented as means ± SEMs. *p < 0.05, **p < 0.01.

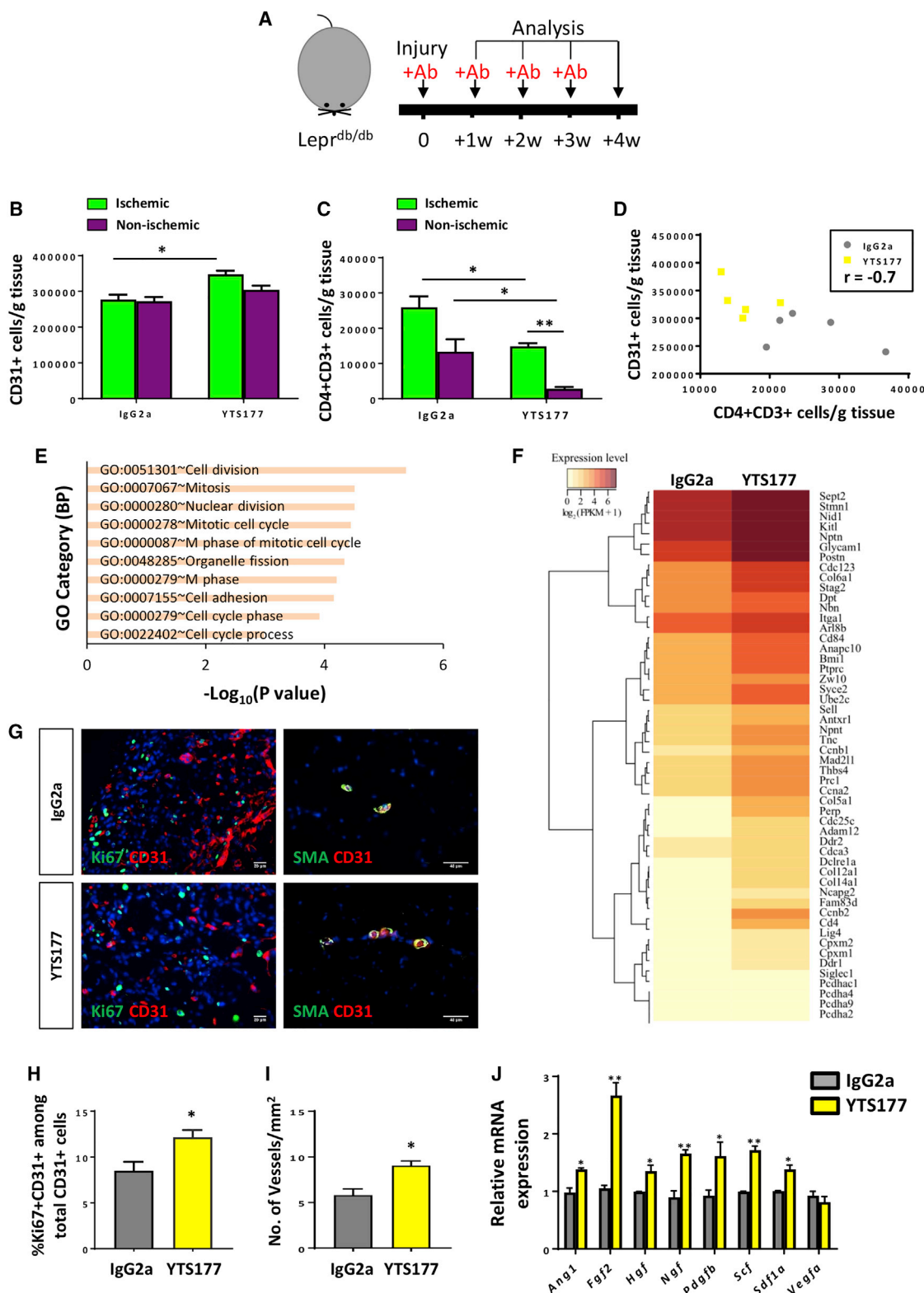


Figure 3. CD4 Coreceptor Blockade Promotes Vascular Regeneration in the Ischemic Tissues of Lepr^{db/db} Mice

(A–C) Schematic diagram showing experimental design (n = 20/group) (A). Flow cytometric quantification showing absolute number of (B) CD31⁺ or (C) CD4⁺(surface and intracellular) CD3⁺ cells/g tissue in the ischemic and non-ischemic muscles after being gated on CD45[−] or CD45⁺ cells, respectively.

(legend continued on next page)

upregulated expression of *Ang1*, *Fgf2*, *Hgf*, *Ngf*, *Pdgfb*, *Scf*, and *Sdf1a* in purified ECs of the YTS177-treated group than of the IgG2a-treated group (Figure 3J). In addition, we observed significantly downregulated gene expression of pro-inflammatory cytokines, including *Il1b*, *Il2*, *Il6*, *Il17*, *Il23a*, and *Tnfa*, in purified ECs of the YTS177-treated group than of the IgG2a-treated group (Figure S6C), suggesting that vascular inflammation in T2D was at least in part mediated by the infiltrating CD4⁺ T cells. Taken together, our findings showed that CD4 coreceptor blockade not only reduced vascular inflammation but also increased vascular and capillary density and promoted endothelial cell proliferation in the ischemic tissues of T2D mice. Dissimilar to normoglycemia, CD4⁺ T cells negatively regulated post-ischemic revascularization in T2D.

CD4 Coreceptor Blockade Enhances Vascular Function in *Lepr^{db/db}*

To examine the role of CD4⁺ T cells in endothelium-dependent vasoreactivity, we performed wire myography in *Lepr^{db/db}* 2 weeks after ischemic injury (Figure 4A). There was significantly augmented acetylcholine (ACh)-induced endothelium-dependent relaxations (EDRs) in the femoral arteries of the ischemic limbs of the YTS177-treated group than of the IgG2a-treated group (Figure 4B). The augmented EDRs in the YTS177-treated group were abolished with the nitric oxide synthase (NOS) inhibitor *N*(G)-nitro-L-arginine methyl ester (L-NAME), suggesting that there was increased endothelial NO bioavailability in the ischemic tissues of T2D mice following CD4 coreceptor blockade. Similarly, there were significantly reduced phenylephrine (Phe)-induced vasoconstrictions (Figure 4C), indicating better EC function in the femoral arteries of the ischemic limbs of the YTS177-treated group than of the IgG2a-treated group. Our results also demonstrated that there were no differences in ACh-mediated EDRs (Figure 4D) or Phe-induced vasoconstrictions (Figure 4E) in the femoral arteries of the non-ischemic limbs of the YTS177- and IgG2a-treated groups, respectively, indicating that the therapeutic effect of YTS177 on enhancing endothelial function was specifically localized to ischemic tissues only.

To elucidate the role of CD4⁺ T cells in functional reperfusion, we performed laser Doppler imaging in *Lepr^{db/db}* weekly for 4 weeks post-ischemic injury (Figure 4F). Our results showed a significant improvement in blood reperfusion in the ischemic limbs of the YTS177-treated group than of the IgG2a-treated group in a dose-dependent manner (Figure 4G). Taken together, our findings showed that CD4 coreceptor blockade improved post-ischemic vascular function in T2D.

CD4 Coreceptor Blockade Enhances Vascular Regeneration and Function in *Lepr^{db/db}* via Tregs

Recently, Tregs were demonstrated to promote wound healing and organ regeneration (Li et al., 2018). To examine whether CD4 coreceptor blockade induced functional revascularization through Tregs, we functionally depleted Tregs via a lytic anti-CD25 mAb (clone PC61), as previously described (Lui et al., 2010; Setiady et al., 2010; Weirather et al., 2014). We asked whether YTS177 and PC61 alter the number of activated CD4⁺ T cells and T cell subsets in the ischemic tissues of T2D. Our flow cytometric analysis showed that YTS177 significantly reduced the absolute number of CD4⁺CD3⁺CD25⁺FOXP3[−] activated T cells in ischemic tissues compared to that of the IgG2a-treated group (Figure 5A). Moreover, we performed intracellular cytokine staining on CD4⁺ T cells and found that YTS177 significantly reduced while PC61 did not alter the number of cytokine-expressing T cells, including IFN- γ , TNF- α , IL-4, IL-6, or IL-17, in ischemic tissues compared to that of IgG2a; this indicated that YTS177 reduced and PC61 did not alter the population of Th1, Th2, or Th17 subsets after injury (Figure 5B). Furthermore, both YTS177 and PC61 treatments significantly reduced the absolute number of CD4⁺CD3⁺CD25⁺FOXP3⁺ Tregs (Figure 5C) and the ratio of Tregs to activated T cells compared to IgG2a (Figure 5D). Our results demonstrated that YTS177 reduced both activated and Tregs and PC61 specifically depleted Tregs in ischemic tissues.

We asked whether CD4 coreceptor blockade enhanced Treg function in ischemic tissues for facilitating vascular regeneration. We performed laser Doppler imaging to assess vascular function following CD4 coreceptor blockade in the absence of Tregs (Figure 5E). Our results demonstrated that YTS177-mediated reperfusion in ischemic tissues was abolished following PC61 treatment at all indicated time points within 4 weeks post-ischemia (Figure 5F), suggesting that CD4 coreceptor blockade-induced functional revascularization in T2D was promoted through Tregs.

CD4 Coreceptor Blockade Enhances Vascular Regeneration and Function in DIO Mice

In addition to *Lepr^{db/db}*, we used lineage-tracing diet-induced obese (DIO) mice as an independent T2D model (Figure 6A). Impaired glucose tolerance was confirmed by the glucose tolerance test (GTT) (Figure 6B). Because DIO mice were at least 3 months older than *Lepr^{db/db}* mice following treatment with a high-fat diet before ischemic injury, we observed a more severe PAD phenotype such as autoamputation. Nevertheless, autoamputation was reduced by 5-fold after YTS177 treatment

(D) Scatterplots showing a negative correlation between EC density and CD4⁺ T cell infiltration into the ischemic muscles of IgG2a-treated and YTS177-treated *Lepr^{db/db}*.

(E and F) Genome-wide RNA-seq results showing (E) the top 10 significant biological processes as determined by upregulated genes expressed by CD45⁺CD31⁺ ECs purified from the ischemic muscles of YTS177-treated as compared to IgG2a-treated mice, and (F) differentially expressed genes on a heatmap as determined by GO functional clustering.

(G–I) (G) Immunostaining on frozen sections, scale bars: 20 μ m and (H and I) quantification for Ki67⁺ (green) or SMA⁺ (green; scale bars: 40 μ m) with CD31⁺ (red) cells and nuclear DAPI counterstain (blue) showing a significantly increased number of (H) Ki67⁺CD31⁺ ECs or (I) SMA⁺CD31⁺ blood vessels per unit area in the ischemic muscles of YTS177-treated than IgG2a-treated mice.

(J) Quantitative RT-PCR of CD45⁺CD31⁺ ECs purified from ischemic muscles by flow cytometry. Gene expression levels in YTS177-treated compared to IgG2a-treated mice.

All data (B–D, H–J) are presented as means \pm SEMs. * $p < 0.05$, ** $p < 0.01$.

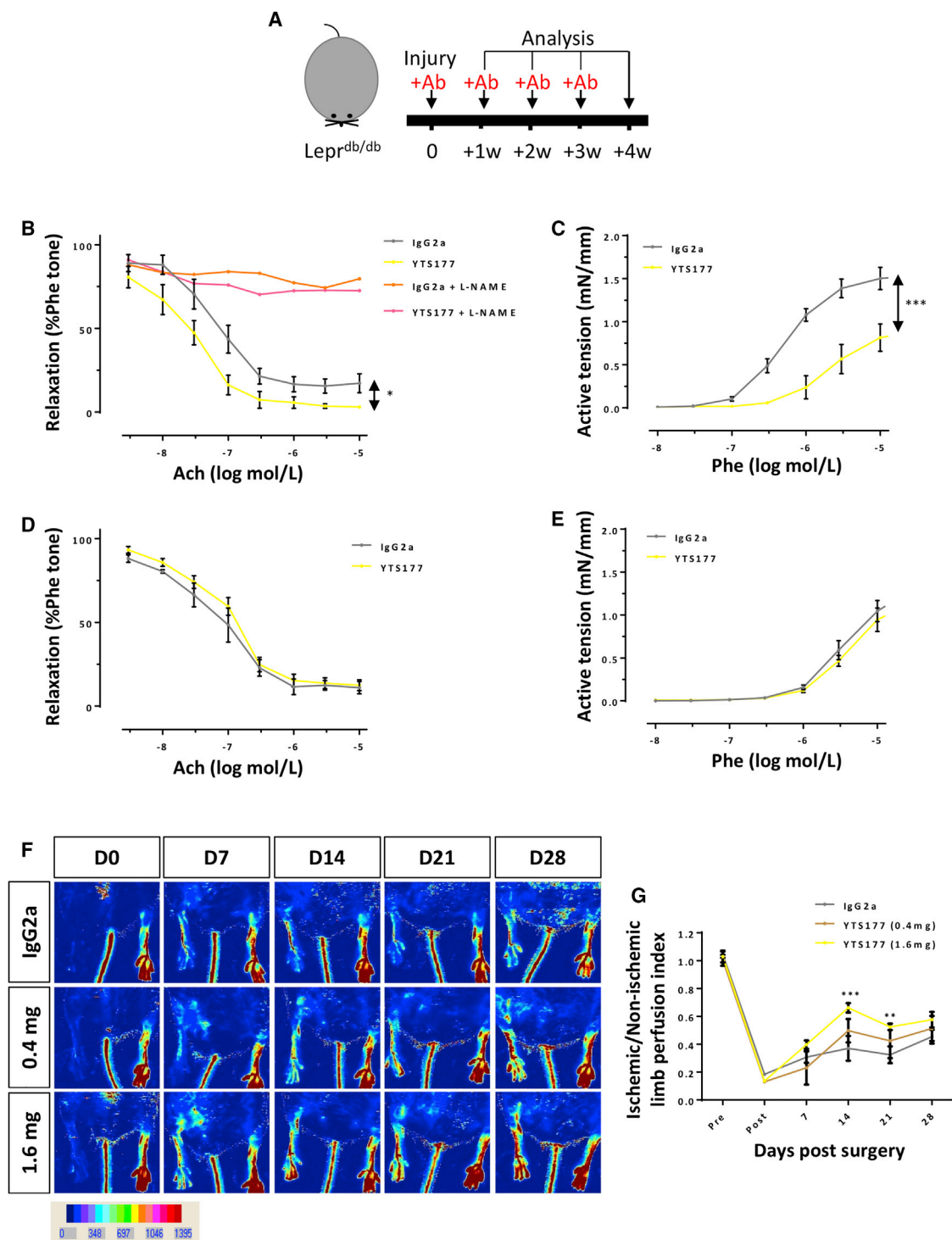


Figure 4. CD4 Coreceptor Blockade Promotes Endothelial Cell Function in the Ischemic Tissues of Lepr^{db/db} Mice

(A) Schematic diagram showing experimental design (n = 6–20/group).

(B–E) Concentration-dependent EDRs of mouse femoral arteries of the (B) ischemic or (D) non-ischemic limbs to ACh were measured after treatment with IgG2a or YTS177, respectively. (B) EDRs were antagonized by co-treatment with the NO synthase (NOS) inhibitor L-NAME. (C and E) Concentration-dependent vasoconstrictions of mouse femoral arteries of the (C) ischemic or (E) non-ischemic limbs to Phe were measured after treatment with IgG2a or YTS177, respectively.

(legend continued on next page)

(4 in 10 IgG2a versus 1 in 13 YTS177; Figure 6C). To determine whether CD4 coreceptor blockade also promoted functional reperfusion in DIO mice, we performed laser Doppler imaging weekly for 4 weeks post-ischemic injury. Consistent with the results in *Lepr^{db/db}* (Figure 4F), we showed significant improvement in blood reperfusion in the ischemic limbs of the YTS177-treated group than of the IgG2a-treated group (Figures 6D and 6E). Taken together, our findings showed that CD4 coreceptor blockade improved post-ischemic vascular function in two independent T2D models.

To examine whether the therapeutic effect of YTS177 was specific to ECs, we performed fate mapping for ECs via *Cdh5-CreER*, in addition to immunostaining for CD31. The genetic lineage-tracing *Cdh5-CreER;Rosa26^{YFP/+}* (YFP, yellow fluorescent protein) mice were treated with tamoxifen at the indicated time points, as previously described (He et al., 2017), to label all ECs before ischemic injury (Figure 6A). Our quantitative results by flow cytometry showed a significant loss of YFP⁺CD31⁺ ECs in ischemic than in the non-ischemic muscles of the IgG2a-treated group but not the YTS177-treated group; there was a significant increase in %YFP⁺CD31⁺ ECs in the ischemic muscles of the YTS177-treated than of the IgG2a-treated group (Figures 6F and 6G). Notably, there was a significant increase in %YFP⁺CD31⁺ cells in the ischemic than in the non-ischemic muscles of the IgG2a-treated group and a significant increase in %YFP⁺CD31⁺ cells in the ischemic muscles of the IgG2a-treated group than of the YTS177-treated group (Figures 6F and 6H). In fact, a previous report showed that CD144⁺CD31⁺ cells developed before the maturation of CD144⁺CD31⁺ ECs during differentiation of ESCs (Orlova et al., 2014). Therefore, the YFP⁺CD31⁺ cells found in the ischemic muscles of the IgG2a-treated group could be immature ECs with reduced or impaired endothelial function.

CD4 Coreceptor Blockade Facilitates Apelin-Mediated Sprouting Angiogenesis via Tregs

Previous work shows that pre-existing ECs form new blood vessels and mediate cardiac neovascularization through sprouting angiogenesis after ischemia (Liu et al., 2015; He et al., 2017). We then asked whether Tregs facilitated sprouting angiogenesis in the ischemic tissues of T2D mice. Accumulating evidence demonstrates that APLN is a marker for sprouting angiogenesis because hypoxia induces APLN expression that regulates EC proliferation and angiogenesis during cardiovascular regeneration (Eyries et al., 2008; Kidoya et al., 2010; Tempel et al., 2012). We, therefore, used the genetic lineage-tracing *Apln-CreER* line to study the role of Tregs in sprouting angiogenesis after ischemic injury in T2D. *Apln-CreER;Rosa26^{YFP/+}* mice were treated with a high-fat diet for 3 months to induce T2D before ischemic injury and were induced with tamoxifen at days 0 and 2 post-ischemia to label all sprouting ECs (Liu et al., 2015) (Figure 7A). To examine whether active sprouting

angiogenesis was completed 4 weeks after ischemia, we performed immunostaining for the estrogen receptor (ESR) to detect CreER, a surrogate for active APLN expression (Liu et al., 2015). While we barely observed sprouting ESR⁺CD31⁺ ECs in the non-ischemic muscles of both groups, there were significantly reduced ESR⁺CD31⁺ sprouting ECs in the ischemic muscles of the YTS177+PC61-treated than in the YTS177-treated mice (Figures 7B and 7C), suggesting that active sprouting angiogenesis took place only in the presence of Tregs following CD4 coreceptor blockade. To investigate the accumulative event of sprouting angiogenesis since the beginning of ischemic injury, we quantified YFP expression among CD45⁺CD31⁺ cells by flow cytometry (Figure 7D). As expected, YFP⁺CD31⁺ sprouting ECs were found in ischemic but scarcely in non-ischemic muscles (Figure 7E). Following ischemia, there were significantly reduced %YFP⁺CD31⁺ sprouting ECs in the YTS177+PC61-treated group than in the YTS177-treated group (Figure 7E), suggesting that Tregs facilitated the induction of APLN expression by ECs, thereby driving sprouting angiogenesis in T2D.

Tregs Directly Promote Angiogenesis in Hyperglycemia in a Paracrine Manner

To ask whether Tregs directly regulated angiogenesis in hyperglycemic conditions, we have performed co-culture experiments with Tregs and ECs at 25 mM D-glucose *in vitro* (Figure S7). Our results showed that mouse ECs failed to form tubes, yet Tregs, conditioned medium of Treg, or Treg-related paracrine factors, including IL-10 and amphiregulin (AREG), significantly promoted tube formation (Figure S7A) and increased total tubule length compared to the PBS control (Figure S7C). We also performed immunostaining for Ki67 and CD31 to assess whether Tregs exerted any mitogenic effects on ECs (Figure S7B). Our results showed that Tregs, IL-10, or AREG increased the total number of CD31⁺ cells (Figure S7D), but only Tregs or IL-10 enhanced the total number of Ki67⁺CD31⁺ cells (Figure S7E). In fact, AREG significantly reduced EC proliferation, indicating that AREG mediated angiogenesis via another mechanism. Moreover, we found that Tregs, IL-10, or AREG significantly enhanced *Apln* gene expression (Figure S7F), which is in line with our *in vivo* studies (Figure 7). To ask whether Treg directly regulated angiogenesis in humans, we performed co-culture experiments with hESC-ECs. Our results showed that IL-10 or AREG significantly promoted tube formation at 25 mM D-glucose *in vitro* (Figures S7G and S7H). In summary, our results showed that Tregs or Treg paracrine factors directly regulated angiogenesis in both mouse and human settings.

DISCUSSION

There is an increasing incidence of PAD as a result of the growing epidemic of obesity and diabetes. Because of complications associated with diabetes, including atherosclerosis, vascular

(F and G) (F) Laser Doppler images and (G) quantification of the ischemic and non-ischemic limb perfusion index showing a dose- and time-dependent dynamic change in the blood flow of YTS177-treated (a total of 0.4 mg from 0.1 mg once weekly for 4 weeks or a total of 1.6 mg from 0.4 mg once weekly for 4 weeks) than IgG2a-treated mice.

All data (B–E and G) are presented as means ± SEMs. *p < 0.05, **p < 0.01, and ***p < 0.001.

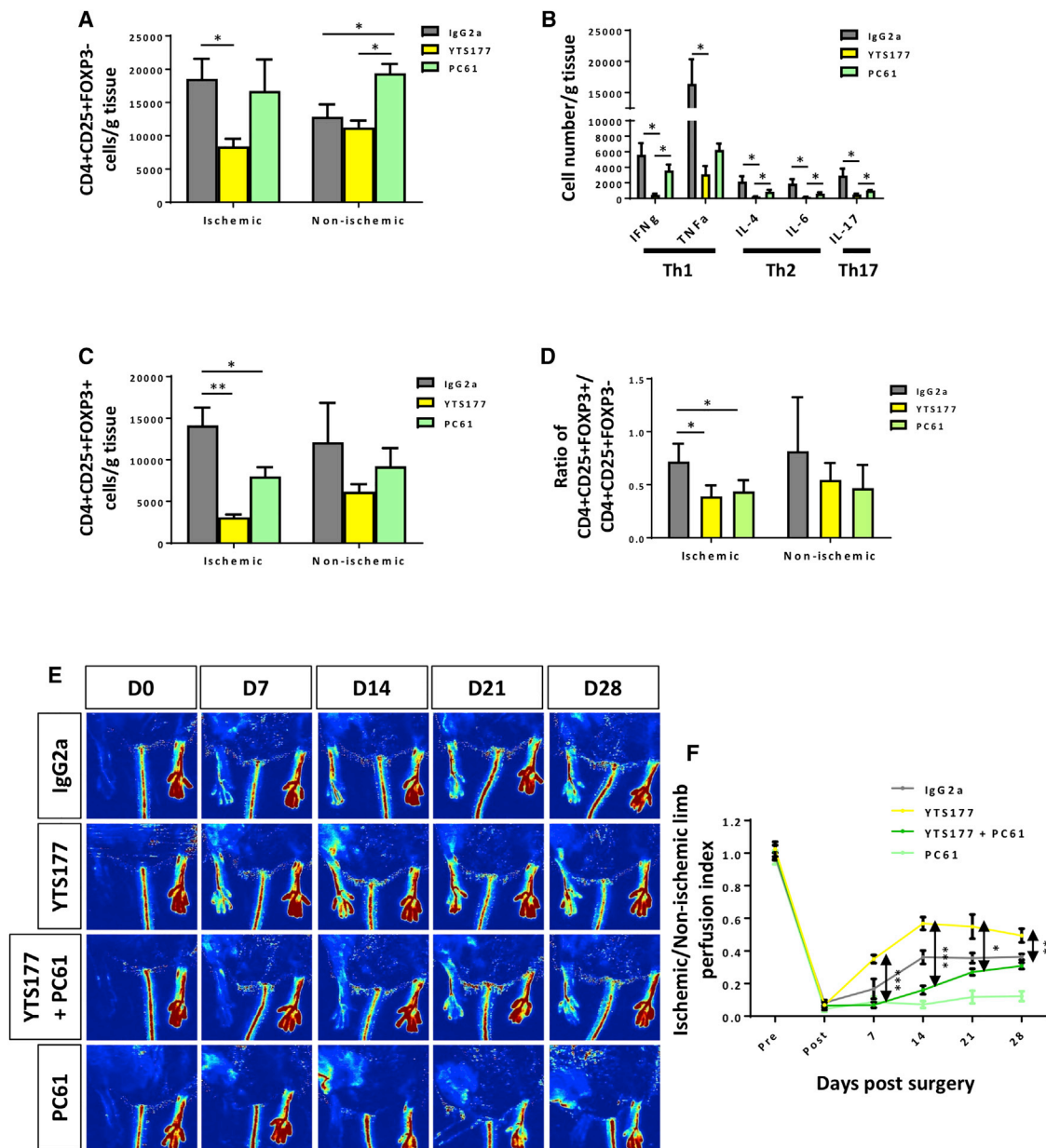


Figure 5. CD4 Coreceptor Blockade Promotes Vascular Regeneration and Function in *Lep^{db/db}* Mice via Tregs

(A–D) Flow cytometric quantification showing the absolute number per gram tissue of (A) CD4⁺(surface and intracellular)CD25⁺FOXP3⁺ activated T cells, (B) various CD4⁺ T cell subsets, (C) CD4⁺(surface and intracellular)CD25⁺FOXP3⁺ Treg, or (D) the ratio of CD4⁺CD25⁺FOXP3⁺ Treg to CD4⁺CD25⁺FOXP3⁺ activated T cells in the ischemic and non-ischemic muscles of IgG2a-, YTS177-, or PC61-treated *Lep^{db/db}*, respectively.

(E and F) (E) Laser Doppler images and (F) quantification of the ischemic and non-ischemic limb perfusion index showing a time-dependent dynamic change in the blood flow of YTS177-, YTS177+PC61-, or PC61-treated compared to IgG2a-treated mice.

All data (A–D and F) are presented as means \pm SEMs; n = 6/group. *p < 0.05, **p < 0.01, and ***p < 0.001.

inflammation, and endothelial dysfunction, trials targeting diabetic PAD have largely failed. The present study aimed to understand the cellular and molecular signatures of diabetic PAD and to report the unappreciated role of CD4⁺ effector cells and Tregs in modulating regeneration of the peripheral artery system in T2D. By collecting the amputated limbs from both normoglycemic and T2D patients with PAD, we found increased numbers

of infiltrating CD4⁺ T cells, particularly Th1 cells, and reduced vascular density in the ischemic tissues of T2D patients than of normoglycemic patients. We also observed the same negative correlation in T2D mice after hindlimb ischemia. In fact, previous reports reveal that autoreactive CD4⁺ T cells infiltrate injured tissues to facilitate healing of the peripheral vascular (Stabile et al., 2003, van Weel et al., 2007, Hata et al., 2011), cardiovascular

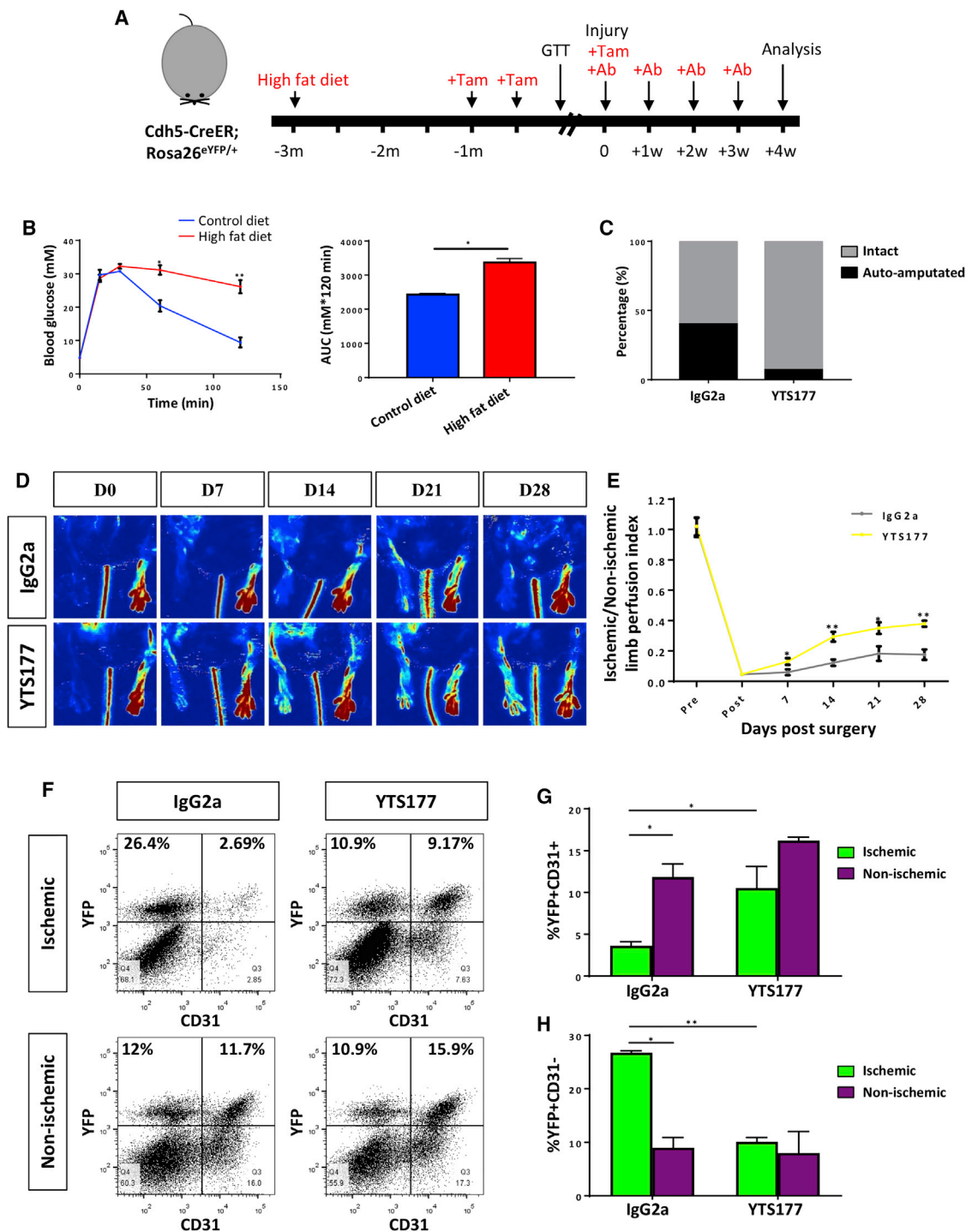


Figure 6. CD4 Coreceptor Blockade Enhances Vascular Regeneration and Function in DIO Mice

(A) Schematic diagram showing experimental design using *Cdh5-CreER;Rosa26^{eYFP/+}* DIO mice (n = 6/group).

(B) GTT results showing insulin resistance after feeding with a high-fat diet for 3 months.

(C) Quantification of autoamputated limbs post-ischemic injury in IgG2a-treated (n = 10) or YTS177-treated (n = 14) mice.

(D and E) (D) Laser Doppler images and (E) quantification of the ischemic and non-ischemic limb perfusion index showing a time-dependent dynamic change in the blood flow of YTS177-treated compared to IgG2a-treated mice.

(legend continued on next page)

(Hofmann et al., 2012), and central nervous systems (Moalem et al., 1999) in normoglycemic models. Whether these tissue-infiltrating CD4⁺ T cells promote healing and *de novo* formation of new blood vessels after ischemic injury in T2D remains unknown.

To address this question, we blocked proliferation, activation, and infiltration of CD4⁺ T cells into the ischemic tissues of T2D mice using a non-lytic anti-CD4 mAb. If the infiltrating CD4⁺ T cells were essential for post-ischemic revascularization in T2D, similar to normoglycemia, then we would observe impaired angiogenesis and endothelial dysfunction after CD4 coreceptor blockade. We used two T2D models in this study: transgenic *Lepr^{db/db}* and DIO mice, the latter being more physiologically relevant to human T2D. Following CD4 coreceptor blockade, the results of genome-wide transcriptomic profiling and immunohistochemistry showed enhanced EC proliferation, and *Cdh5-CreER* lineage-tracing experiments revealed significantly increased CDH5⁺CD31⁺ mature ECs in ischemic tissues. Furthermore, wire myography and laser Doppler data demonstrated enhanced vasoreactivity such as EDRs, increased endothelial NO production, and increased blood reperfusion in ischemic tissues. Collectively, our findings revealed that CD4 coreceptor blockade significantly promoted rather than reduced EC proliferation and function after ischemic injury in both *Lepr^{db/db}* and DIO mice. Therefore, tissue-infiltrating CD4⁺ T cells contributed to impaired vasculogenesis and endothelial dysfunction in T2D. Nevertheless, it is unclear whether other T cell subsets also regulate vascular regeneration. In fact, we observed the CD4⁺CD3⁺ population in the ischemic tissues of both patients and the analogous mouse models. It requires future investigations into their role and functional relation with CD4⁺ T cells in modulating ischemic injury in T2D.

Immune-mediated tissue repair is an emerging paradigm in the field of regenerative medicine. A large body of evidence highlights the importance of macrophages in tissue repair and regeneration (Wynn and Vannella, 2016; Eming et al., 2017). Nevertheless, whether adaptive immune cells such as T cells contribute to tissue regeneration is less studied. In fact, targeting T cells for tissue regeneration offers unique advantages such as long-term therapeutic efficacy because of T cell memory and specificity toward autoantigens released during injury. We observed that vascular regeneration via CD4 coreceptor blockade was localized in the ischemic but not the non-ischemic tissues. Recently, CD4⁺ Tregs were shown to play a direct or an indirect role in tissue repair and regeneration. Weirather et al. (2014) show that Tregs indirectly improve the healing of heart muscle after myocardial infarction by modulating the differentiation of pro-regenerative M2 macrophages. Burzyn et al. (2013) also reveal that Tregs directly promote satellite cell activation and skeletal muscle regeneration via AREG production, and Arpaia et al. (2015) demonstrate that Tregs facilitate tissue repair after

influenza infection. Moreover, Dombrowski et al. (2017) note that Tregs promote oligodendrocyte differentiation and myelin regeneration in the central nervous system, and Ali et al. (2017) reveal that Tregs facilitate proliferation and differentiation of hair follicular stem cells in skin. Nevertheless, whether Tregs regulate regeneration of the peripheral vascular system remains unclear.

In this study, we observed that the ischemic tissues of T2D patients or *Lepr^{db/db}* mice had a significantly reduced number of CD4⁺CD25⁺FOXP3⁺ Treg compared to their normoglycemic counterparts. Treatment with CD4 coreceptor blockade also reduced the ratio of Tregs to activated T cells in ischemic tissues, given that we considered all CD4⁺ T cells, including those that had internalized (intracellular) CD4 molecules. We found, albeit with a smaller amount, that the vascular regenerative effect of CD4 coreceptor blockade was mediated by Tregs because functional reperfusion following immunotherapy was abolished with PC61 treatment that specifically and functionally depletes CD4⁺CD25^{hi} Tregs. One limitation in relating T cell quantity to function is that we assumed that all CD4-expressing T cells were functional. However, conventional CD4⁺ T cells that internalized CD4 molecules could be less likely to exert effector function because they require CD4 to interact with antigen-presenting cells in response to neoantigens during ischemic injury. If conventional CD4⁺ T cells were to use LAG3 in the replacement of CD4 for antigen recognition, their proliferation and activation could also be inhibited because ectopic expression of LAG3 on CD4⁺ T cells significantly reduces their proliferative activity and confers on them suppressor activity (Huang et al., 2004). Alternatively, Tregs can bind to antigens via LAG3 instead of CD4, and LAG3 enhances the regulatory function of Tregs (Do et al., 2016). Therefore, it is possible that Tregs may consequently have an operational advantage when CD4 is internalized. It has also been reported that YTS177 alone facilitates Treg function during the induction of immune tolerance to skin allografts (Cobbald et al., 2004).

Furthermore, in our genetic lineage-tracing experiments using *ApIn-CreER*, we specifically demonstrated that Tregs potentiated the *de novo* formation of new blood vessels through regulating apelin expression as depletion of Treg via PC61 downregulated apelin expression in ECs that drives functional sprouting angiogenesis in ischemic tissues (Eyries et al., 2008; Kidoya et al., 2010; Tempel et al., 2012). Our *in vitro* angiogenesis assays also showed that Tregs operated in a paracrine manner as conditioned medium or factors derived from Tregs such as IL-10 or AREG promoted tube formation. Tregs or IL-10 directly promoted EC proliferation, and Tregs, IL-10, or AREG facilitated apelin expression. Nevertheless, the signals that activated Treg recruitment into ischemic tissues remain unknown. In future follow-up studies, one could perform a genome-wide search in a single-cell resolution coupled with flow cytometric analysis and loss-of-function studies *in vivo*

(F–H) (F) Dot plots and (G and H) quantification of cell populations in the ischemic and non-ischemic muscles showing (G) significantly increased %YFP⁺CD31⁺ mature ECs in the ischemic muscles of YTS177-treated than IgG2a-treated mice, and (H) significantly reduced %YFP⁺CD31⁺ immature ECs in the ischemic muscles of YTS177-treated than IgG2a-treated mice.

All data (B, E, G, and H) are presented as means ± SEMs. *p < 0.05, **p < 0.01.

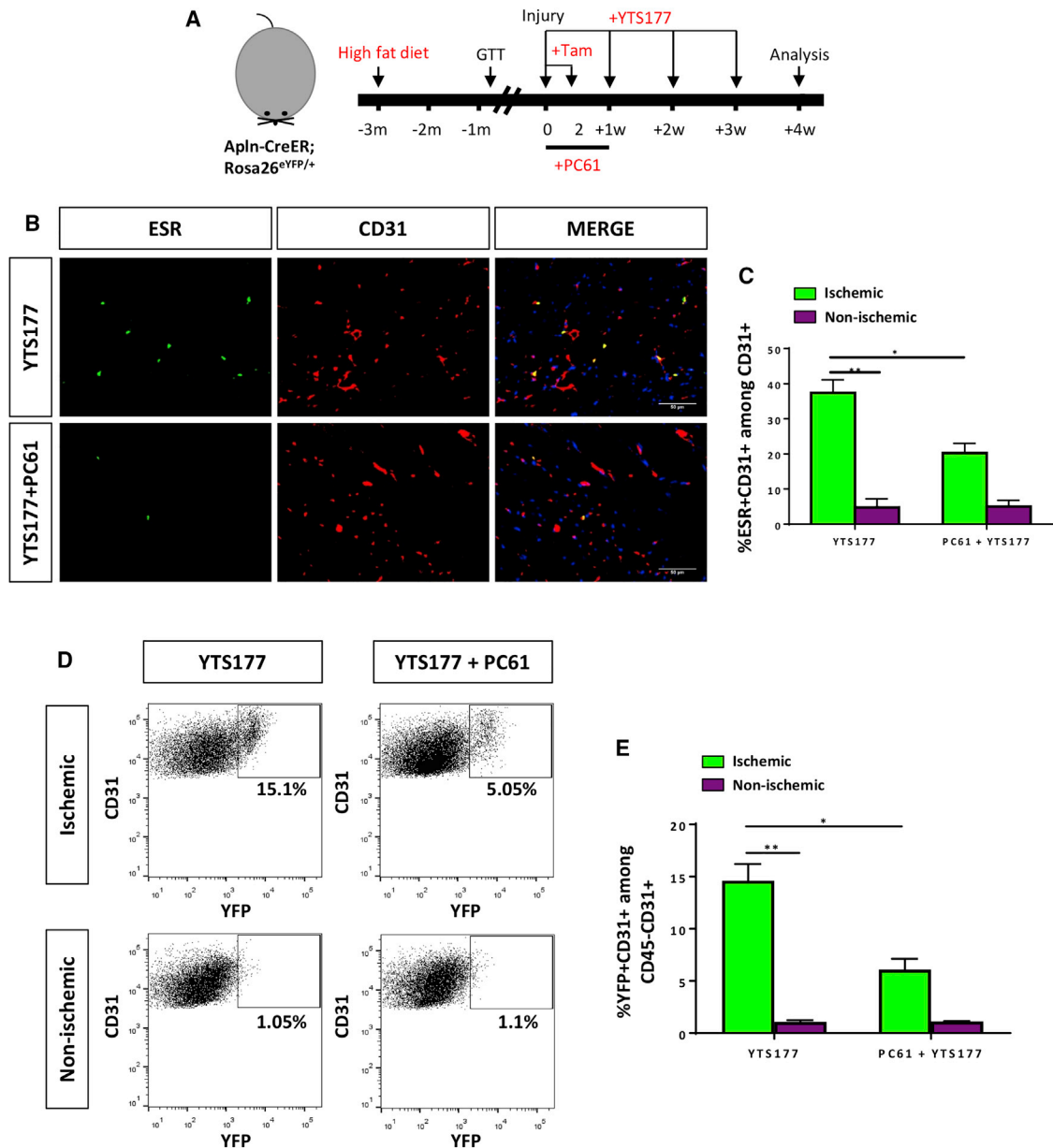


Figure 7. CD4 Coreceptor Blockade Promotes Apelin-Mediated Sprouting Angiogenesis in DIO Mice via Tregs

(A) Schematic diagram showing experimental design using *Apln-CreER; Rosa26^{YFP/+}* DIO mice (n = 6/group).

(B and C) (B) Immunostaining on frozen sections and (C) quantification for ESR⁺ and CD31⁺ cells showing significantly more active sprouting angiogenesis in the ischemic muscles of YTS177-treated than YTS177+PC61-treated mice. Scale bars: 50 μ m.

(D and E) (D) Dot plots and (E) quantification among CD45⁺CD31⁺ cells in the ischemic and non-ischemic muscles showing significantly reduced %YFP⁺CD31⁺ sprouting ECs in the ischemic muscles of YTS177+PC61-treated than YTS177-treated mice.

All data (C and E) are presented as means \pm SEMs. *p < 0.05 and **p < 0.01.

to determine signals that activate local Tregs for driving vascular regeneration in T2D.

Taken together, our results address a long-standing question of why diabetic humans (Simons, 2005) and mice lack functional revascularization post-ischemia, even though there is clear evidence of the infiltration and activation of CD4⁺ T cells known to promote vascular function in normoglycemia. We have high-

lighted a hitherto novel role of CD4⁺ T cells in impairing vasculogenesis and a regenerative role of Tregs in promoting *de novo* functional sprouting angiogenesis in T2D by stimulating EC proliferation and upregulating apelin expression in the ECs of ischemic tissues. Our findings offer new avenues for developing novel therapeutics targeting Treg-mediated regeneration of the peripheral artery system in obesity and diabetes.

EXPERIMENTAL PROCEDURES

Human Patients

All of the procedures were approved by The Chinese University of Hong Kong (CUHK) Hospital Authority Clinical Research Ethics Committee. Samples were collected after below-the-knee amputations from the gastrocnemius muscles of 8 normoglycemic and 12 T2D patients with PAD (Table S1). Patients with infections were excluded to prevent interference in immune cell analysis.

Mice

All of the procedures were approved by the CUHK Animal Experimentation Ethics Committee. Male adult *Lepr^{db/db}* and *Lepr^{db/+}* mice were purchased from Jackson Laboratory. *Foxp3^{hCD2}* reporter (Miyao et al., 2012), *Cdh5-CreER* (He et al., 2017), and *Apln-CreER* (Liu et al., 2015) were generated, as described previously. For Cre induction, tamoxifen was dissolved in corn oil (20 mg/mL) and administered by oral gavage (0.15 mg tamoxifen/g body weight) at the indicated time points. Specifically, *Cdh5-CreER;Rosa26^{YFP/+}* was treated with tamoxifen at week -4 and -2 pre-ischemia and day 0 post-ischemia, and *Apln-CreER;Rosa26^{YFP/+}* was treated with tamoxifen at day 0 and 2 post-ischemia. A high-fat diet (60% fat, Envigo) was fed for at least 4 months to induce DIO. The GTT was performed with D-glucose (2 g/kg body weight) injected intraperitoneally (i.p.) following 16 hr of fasting.

Cell Cultures

Naive CD4⁺hCD2⁺ Tregs were purified from the spleen of *Foxp3^{hCD2}* by flow cytometry and activated *in vitro* by anti-CD3 (Biolegend), anti-CD28 (Biolegend), 40 ng/mL IL-2 (Peprotech), and 10 ng/mL transforming growth factor (TGF- β) (RnD Systems), as described previously (Fantini et al., 2007). After that, Tregs were used for co-culture experiments with mouse ECs in a ratio of EC:Treg at 2:1 after 4–5 days of activation. Mouse ECs were isolated from the aorta of 5-week-old mice, as described previously (Tian et al., 2012a), and cultured in EGM-2 medium (Lonza) containing 25 mM D-glucose (Sigma) for 3 days in the presence of Tregs, conditioned medium of Treg (in EGM-2), or Treg-derived factors such as 50 ng/mL IL-10 (Biolegend) or 50 ng/mL AREG (Peprotech). For hESC cultures, H9 ESCs (WiCell) were maintained in mTeSR1 medium (Stemgent) and differentiated into hESC-ECs with a protocol modified from a previous report (Patsch et al., 2015). Briefly, hESCs were cultured in mesoderm differentiation medium containing 50% DMEM/F12 and 50% neurobasal media supplemented with 1% N2, 2% B27, and 50 μ M 2-mercaptoethanol. Growth factors and small molecules, including 8 μ M CHIR 99021 (Selleckchem) and 25 ng/mL BMP4 (Peprotech), were added to mesoderm differentiation medium at days 1–4. At days 4–7, hESCs were cultured in EC differentiation medium containing StemPro-34 SFM medium (Life Technologies) supplemented with 1% GlutaMAX (Thermo Fisher Scientific), 200 ng/mL VEGF-A (Peprotech), and 2 μ M Forskolin (Abcam). At days 7–10, CD31⁺CD144⁺ hESC-ECs were purified by flow cytometry and maintained to mature in StemPro-34 SFM medium supplemented with 1% GlutaMAX and 50 ng/mL VEGF-A. At days 10–18, mature hESC-ECs were cultured in 25 mM glucose (L or D, Sigma), with the last 3 days in the presence of cytokines, including 10 ng/mL IFN- γ , 50 ng/mL TNF- α , 50 ng/mL IL-10, or 50 ng/mL AREG (all Peprotech).

Tube Formation Assay

A total of 15,000 mouse aortic ECs or hESC-ECs were plated into each well of a 96-well plate with 50 μ L Matrigel (BD Biosciences). Images were taken after 20 hr of cultures and analyzed by ImageJ with the Angiogenesis Analyzer plug-in for the quantification of tube networks and total tubule length.

Severe Hindlimb Ischemia

Mice were anesthetized with ketamine (100 mg/kg) and xylazine (10 mg/kg). Unilateral ischemia was induced by ligating the femoral artery at two points proximal and distal to the bifurcation of the superficial and the deep femoral arteries, followed by excision of the intervening segment (Krishna et al., 2016).

Administration of mAbs

Non-lytic anti-CD4 mAbs (clone YTS177) were generated, as described previously (Qin et al., 1989, 1990). We i.p. injected 0.4 mg IgG2a (isotype control) or

anti-CD4 mAb once weekly for 4 weeks post-ischemia, and 1 mg lytic anti-CD25 mAb (clone PC61, BioxCel) was i.p. injected on days 0, 2, and 4 post-ischemia, as described previously (Lui et al., 2010).

Skeletal Muscle/Single-Fiber and EC Isolation

The quantification of EC density and immune infiltrates was examined after single-fiber isolation, as described previously (Zhou et al., 2015). For mice, the muscles of the femur were minced and enzymatically digested in buffer D containing 1000 U/mL collagenase II (Worthington) and 1% penicillin/streptomycin (Pen/Strep) (GIBCO) in F10 medium (Sigma) at 37°C for 1.5 hr with agitation. Muscle cells were washed with 10% horse serum (GIBCO) and 1% Pen/Strep (GIBCO) in F10 medium and further digested with 11 U/mL dispase (GIBCO) and 1000 U/mL collagenase II at 37°C for 0.5 hr with agitation. For patients, gastrocnemius muscles were minced and digested in buffer D. Two rounds of agitated digestion were needed with each at 37°C for 1 hr. For ECs, the lumen of human arteries was first washed with PBS and incubated in buffer D at 37°C for 1 hr with agitation. Afterward, ECs were flushed out with PBS and washed with fetal bovine serum (FBS)-containing medium.

Flow Cytometry and Cell Sorting

Red blood cells were first removed with lysis buffer (eBiosciences) at room temperature for 5 min. For human tissues, the dissociated mixtures of muscle cells and immune infiltrates or ECs were blocked with 2% serum and incubated with fluorochrome-conjugated antibodies at 4°C for 30 min. For mouse tissues, the dissociated mixture of muscle cells, ECs, and immune infiltrates were first incubated with 2% rat serum, followed by staining with fluorochrome-conjugated antibodies at 4°C for 30 min. For intracellular staining, dissociated cells were re-stimulated *in vitro* at 37°C for 6 hr in the presence of ionomycin (1 μ g/mL, Sigma), phorbol-12-myristate-13-acetate (50 ng/mL, Sigma), and brefeldin A (BD Biosciences). After that, intracellular staining was achieved by a staining kit per the manufacturer's instructions (eBiosciences). For human or mouse tissues, we targeted the following antigens: CD2, CD3, CD4 (clone RM4-4 for mouse CD4), CD25, CD31, CD45, CD144, FOXP3, IL-4, IL-6, IL-17, IFN- γ , and TNF- α (BD Biosciences or Biolegend). Cells were then washed three times with 2% FBS-containing PBS and analyzed on a flow cytometer (BD FACSAria Fusion). Propidium iodide (PI, BD Pharmingen)-positive dead cells were excluded from live cell analysis or sorting, and fluorescence-activated cell sorting (FACS) data were analyzed by the FlowJo software (Tree Star). Because the same weight of the dissected muscles of *Lepr^{db/db}* contained more fat than *Lepr^{db/+}*, the absolute cell number per gram tissue was also normalized to the same cell number after muscle dissociation, during which adipocytes were removed when we compared *Lepr^{db/+}* and *Lepr^{db/db}*.

Immunostaining and Confocal Microscopy

Briefly, muscles were collected in cold PBS and fixed in 4% paraformaldehyde at 4°C for 1 hr. After washing in PBS, muscles were equilibrated in 30% sucrose at 4°C overnight before freezing in optimal cutting temperature (OCT) for cryosectioning. Sections of 6 μ m were blocked with 0.1% Triton X-100/2% goat serum at room temperature for 1 hr, followed by incubation of primary antibodies (CD31, BD Biosciences; YFP, Abcam; ESR, Abcam; Ki67, Abcam; SMA, R&D Systems) at 4°C overnight. Alexa Fluor-conjugated secondary antibodies (Invitrogen) were used at 4°C for 30 min and nuclear counterstain DAPI (Vector Labs) was used at room temperature for 5 min. Slides were mounted with fluorescence mounting medium (Dako) and dried at 4°C overnight in the dark. Fluorescence was detected by confocal microscope (Leica) and analyzed by ImageJ (NIH) with quantification by blind cell counting.

Laser Doppler Imaging

Mice were anesthetized, and blood perfusion was assessed serially at rest with a laser Doppler perfusion imager (Moon Instruments) at days 7, 14, 21, and 28 post-ischemia. Vascularity index as a measure of perfusion (normalized to the muscle area) was quantified and expressed by a ratio of ischemic to non-ischemic limbs, as described previously (Babu et al., 2015).

Wire Myograph

Vasoreactivity was measured in wire myograph, as previously described (Tian et al., 2012b). Femoral arteries were removed and dissected in oxygenated

ice-cold Krebs solution that contained (in mmol/L): 119 NaCl, 4.7 KCl, 2.5 CaCl₂, 1 MgCl₂, 25 NaHCO₃, 1.2 KH₂PO₄, and 11 D-glucose. Measurements of isometric tension were recorded in wire myograph (Danish Myo Technology). The arterial segments were stretched to optimal baseline tension at 1 mN. After that, they were washed in Krebs solution three times and allowed to equilibrate for 1 hr before being contracted with 60 mmol/L KCl to test viability. EDR was measured by testing concentration responses to the cumulative addition of ACh in Phe (3 μmol/L) pre-contracted segments. Some arteries were incubated with NO synthase inhibitor L-NAME (100 μmol/L, 30 min) before testing vasodilation. Vasoconstriction induced by cumulative concentration of Phe was tested before and after L-NAME, which reflects basal NO production.

Real-Time qPCR

Total RNA was isolated from flow cytometer-sorted live cells using the RNeasy Mini Kit (QIAGEN) and reverse transcribed using the iScript cDNA Synthesis Kit (Bio-Rad), according to the manufacturers' instructions. qPCR was analyzed on the QuantStudio 12K Flex Read-Time PCR system (Thermo Fisher Scientific) via SYBR Green (Bio-Rad). Gene expression was indicated by a relative quantitation value determined by the 2^{-ddCT} method, which represents the fold change normalized to the housekeeping genes β-actin and Gapdh. The relative gene expression level of each sample was compared with an internal control.

RNA-Seq and Functional Annotations

Total RNA was isolated and analyzed on the Agilent Tape station for RNA integrity numbers (RINs) before library preparation. RNA-seq libraries were prepared using the TruSeq Stranded mRNA Library Prep Kit according to the manufacturer's protocol (Illumina). mRNA was isolated using poly-T oligos conjugated to magnetic beads and then fragmented and reverse-transcribed to cDNA. Deoxyuridine triphosphates (dUTPs) were incorporated during second strand synthesis and thus were not amplified. cDNA underwent end-repair, ligation with indexed adapters, and PCR amplification. Nucleic acid was cleaned up after each step using AMPure XP beads (Beckman Coulter). Libraries were quantified, pooled, and sequenced at single-end 50 bp on the Illumina HiSeq platform. Raw sequencing data were demultiplexed and converted into FASTQ files using VASAVA (version 1.8.2). Libraries were sequenced at an average depth of 20 million reads per library. The sequenced reads were aligned to the mouse reference genome (mm9) with an annotated gene model file (refSeq 20140714) using Tophat (version 2.0.4) (parameters for single reads: -p 20-transcriptome-mismatches 3-bowtie1-genome-read-mismatches 3). Reference genome and gene model file were downloaded from the University of California, Santa Cruz (UCSC) genome browser. The expression abundances of all genes were estimated by running Cufflinks in its expression level estimation mode across all of the samples. The differential expression analysis was performed using an in-house bioinformatics pipeline (Tsui et al., 2014). This pipeline adopts an M-A plot-based method to compare expression levels. For each gene, the M was calculated as the log₂ difference of expression abundance between two conditions, and the A was calculated as the averaged expression abundance in log₂ scale. The M can be binned using a sliding-window size (e.g., 0.0001). If an M element fell in the upper 5th percentile or the lower 5th percentile in the corresponding bin, then the associated genes were considered to be differentially expressed genes. The identified differentially expressed genes in comparison of CD45⁺CD31⁺ ECs isolated from the ischemic tissues of Lepr^{db/db} and Lepr^{db/+} or of YTS177-treated and IgG2a-treated mice were further annotated with GO using the David Bioinformatics Tool (NIH).

Statistics

All of the data were expressed as means ± SEMs with biological replicates, n = 6 unless otherwise specified, performed under the same conditions. Statistical analysis was performed using the two-sided unpaired Student's t test for comparing differences between two groups, while data from over two groups was analyzed by ANOVA followed by Tukey's method for multiple comparisons. Quantification of tube networks and total tubule length was analyzed by a one-way ANOVA with a Dunnett test by comparing each parameter with the PBS control. Significance was accepted when p < 0.05. Correlation

between two variables was determined by the Pearson correlation coefficient calculated using R (R Foundation).

DATA AND SOFTWARE AVAILABILITY

RNA-seq data are deposited on Mendeley with the <https://doi.org/10.17632/4n2whfwvd6.1>.

SUPPLEMENTAL INFORMATION

Supplemental Information includes seven figures and three tables and can be found with this article online at <https://doi.org/10.1016/j.celrep.2018.07.019>.

ACKNOWLEDGMENTS

We thank Dr. Shohei Hori (RIKEN, Japan) for the kind gift of *Foxp3*^{hCD2} mice. We also thank Drs. Sally Cheng and Ronald Wong for their help in patient recruitment and Miss Ethel Ng, Dr. Francis Lam, Mr. Don Chin, Dr. Cai Liang, and Bao Sheng for their technical help. This work was supported by Research Grants Council of Hong Kong (24110515, 14111916, C4024-16W, and C4026-17WF), Health and Medical Research Fund (03140346 and 04152566), Croucher Foundation (Innovation Award and Start-up Allowance), CUHK Direct Grant, Faculty Innovation Award, and Seed Fund from the Lui Chi Woo Institute of Innovative Medicine.

AUTHOR CONTRIBUTIONS

O.M.L., J.L., X.L., V.W.C., M.K., and X.Y.T. performed the experiments. H.S., H.W., Y.H., J.L., and B.Z. contributed the reagents. O.M.L., J.L., X.L., K.Y.Y., L.J., and K.O.L. analyzed the data. K.O.L. designed the research and wrote the manuscript.

DECLARATION OF INTERESTS

The authors declare no competing interests.

Received: December 1, 2017

Revised: June 27, 2018

Accepted: July 5, 2018

Published: August 7, 2018

REFERENCES

- Ali, N., Zirak, B., Rodriguez, R.S., Pauli, M.L., Truong, H.A., Lai, K., Ahn, R., Corbin, K., Lowe, M.M., Scharschmidt, T.C., et al. (2017). Regulatory T cells in skin facilitate epithelial stem cell differentiation. *Cell* 169, 1119–1129.e11.
- Arpaia, N., Green, J.A., Molledo, B., Arvey, A., Hemmers, S., Yuan, S., Treuting, P.M., and Rudensky, A.Y. (2015). A distinct function of regulatory T cells in tissue protection. *Cell* 162, 1078–1089.
- Babu, M., Durga Devi, T., Mäkinen, P., Kaikkonen, M., Lesch, H.P., Juntila, S., Laiho, A., Ghimire, B., Gyenesi, A., and Ylä-Herttuala, S. (2015). Differential promoter methylation of macrophage genes is associated with impaired vascular growth in ischemic muscles of hyperlipidemic and type 2 diabetic mice: genome-wide promoter methylation study. *Circ. Res.* 117, 289–299.
- Burzyn, D., Kuswanto, W., Kolodin, D., Shadrach, J.L., Cerletti, M., Jang, Y., Sefik, E., Tan, T.G., Wagers, A.J., Benoist, C., and Mathis, D. (2013). A special population of regulatory T cells potentiates muscle repair. *Cell* 155, 1282–1295.
- Cobbold, S.P., Castejon, R., Adams, E., Zelenika, D., Graca, L., Humm, S., and Waldmann, H. (2004). Induction of foxP3+ regulatory T cells in the periphery of T cell receptor transgenic mice tolerized to transplants. *J. Immunol.* 172, 6003–6010.
- Couffignal, T., Silver, M., Kearney, M., Sullivan, A., Witzensbichler, B., Magner, M., Annex, B., Peters, K., and Isner, J.M. (1999). Impaired collateral vessel development associated with reduced expression of vascular endothelial growth factor in ApoE^{-/-} mice. *Circulation* 99, 3188–3198.

- Do, J.S., Visperas, A., Sanogo, Y.O., Bechtel, J.J., Dvorina, N., Kim, S., Jang, E., Stohlman, S.A., Shen, B., Fairchild, R.L., et al. (2016). An IL-27/Lag3 axis enhances Foxp3+ regulatory T cell-suppressive function and therapeutic efficacy. *Mucosal Immunol.* 9, 137–145.
- Dombrowski, Y., O'Hagan, T., Dittmer, M., Penalva, R., Mayoral, S.R., Bankhead, P., Fleville, S., Eleftheriadis, G., Zhao, C., Naughton, M., et al. (2017). Regulatory T cells promote myelin regeneration in the central nervous system. *Nat. Neurosci.* 20, 674–680.
- Eming, S.A., Wynn, T.A., and Martin, P. (2017). Inflammation and metabolism in tissue repair and regeneration. *Science* 356, 1026–1030.
- Eyries, M., Siegfried, G., Ciumas, M., Montagne, K., Agrapart, M., Lebrin, F., and Soubrier, F. (2008). Hypoxia-induced apelin expression regulates endothelial cell proliferation and regenerative angiogenesis. *Circ. Res.* 103, 432–440.
- Fantini, M.C., Dominitzki, S., Rizzo, A., Neurath, M.F., and Becker, C. (2007). In vitro generation of CD4+ CD25+ regulatory cells from murine naive T cells. *Nat. Protoc.* 2, 1789–1794.
- Feuerer, M., Herrero, L., Cipolletta, D., Naaz, A., Wong, J., Nayer, A., Lee, J., Goldfine, A.B., Benoist, C., Shoelson, S., and Mathis, D. (2009). Lean, but not obese, fat is enriched for a unique population of regulatory T cells that affect metabolic parameters. *Nat. Med.* 15, 930–939.
- Hata, T., Takahashi, M., Hida, S., Kawaguchi, M., Kashima, Y., Usui, F., Morimoto, H., Nishiyama, A., Izawa, A., Koyama, J., et al. (2011). Critical role of Th17 cells in inflammation and neovascularization after ischaemia. *Cardiovasc. Res.* 90, 364–372.
- He, L., Huang, X., Kanisicak, O., Li, Y., Wang, Y., Li, Y., Pu, W., Liu, Q., Zhang, H., Tian, X., et al. (2017). Preexisting endothelial cells mediate cardiac neovascularization after injury. *J. Clin. Invest.* 127, 2968–2981.
- Hofmann, U., Beyersdorf, N., Weirather, J., Podolskaya, A., Bauersachs, J., Ertl, G., Kerkau, T., and Frantz, S. (2012). Activation of CD4+ T lymphocytes improves wound healing and survival after experimental myocardial infarction in mice. *Circulation* 125, 1652–1663.
- Howard, D.P., Banerjee, A., Fairhead, J.F., Hands, L., Silver, L.E., and Rothwell, P.M.; Oxford Vascular Study (2015). Population-based study of incidence, risk factors, outcome, and prognosis of ischemic peripheral arterial events: implications for prevention. *Circulation* 132, 1805–1815.
- Huang, C.T., Workman, C.J., Flies, D., Pan, X., Marson, A.L., Zhou, G., Hipkiss, E.L., Ravi, S., Kowalski, J., Levitsky, H.I., et al. (2004). Role of LAG-3 in regulatory T cells. *Immunity* 21, 503–513.
- Kidoya, H., Naito, H., and Takakura, N. (2010). Apelin induces enlarged and nonleaky blood vessels for functional recovery from ischemia. *Blood* 115, 3166–3174.
- Kikuchi, R., Nakamura, K., MacLauchlan, S., Ngo, D.T., Shimizu, I., Fuster, J.J., Katanasaka, Y., Yoshida, S., Qiu, Y., Yamaguchi, T.P., et al. (2014). An antiangiogenic isoform of VEGF-A contributes to impaired vascularization in peripheral artery disease. *Nat. Med.* 20, 1464–1471.
- Krishna, S.M., Omer, S.M., and Golledge, J. (2016). Evaluation of the clinical relevance and limitations of current pre-clinical models of peripheral artery disease. *Clin. Sci. (Lond.)* 130, 127–150.
- Li, J., Tan, J., Martino, M.M., and Lui, K.O. (2018). Regulatory T-cells: potential regulator of tissue repair and regeneration. *Front. Immunol.* 9, 585.
- Liu, Q., Hu, T., He, L., Huang, X., Tian, X., Zhang, H., He, L., Pu, W., Zhang, L., Sun, H., et al. (2015). Genetic targeting of sprouting angiogenesis using Apla-CreER. *Nat. Commun.* 6, 6020.
- Lui, K.O., Boyd, A.S., Cobbold, S.P., Waldmann, H., and Fairchild, P.J. (2010). A role for regulatory T cells in acceptance of ESC-derived tissues transplanted across an major histocompatibility complex barrier. *Stem Cells* 28, 1905–1914.
- Lui, K.O., Howie, D., Ng, S.W., Liu, S., Chien, K.R., and Waldmann, H. (2014). Tolerance induction to human stem cell transplants with extension to their differentiated progeny. *Nat. Commun.* 5, 5629.
- McLaughlin, T., Liu, L.F., Lamendola, C., Shen, L., Morton, J., Rivas, H., Winer, D., Tolentino, L., Choi, O., Zhang, H., et al. (2014). T-cell profile in adipose tissue is associated with insulin resistance and systemic inflammation in humans. *Arterioscler. Thromb. Vasc. Biol.* 34, 2637–2643.
- Miyao, T., Floess, S., Setoguchi, R., Luche, H., Fehling, H.J., Waldmann, H., Huehn, J., and Hori, S. (2012). Plasticity of Foxp3(+) T cells reflects promiscuous Foxp3 expression in conventional T cells but not reprogramming of regulatory T cells. *Immunity* 36, 262–275.
- Moalem, G., Leibowitz-Amit, R., Yoles, E., Mor, F., Cohen, I.R., and Schwartz, M. (1999). Autoimmune T cells protect neurons from secondary degeneration after central nervous system axotomy. *Nat. Med.* 5, 49–55.
- Nishimura, S., Manabe, I., Nagasaki, M., Eto, K., Yamashita, H., Ohsugi, M., Otsu, M., Hara, K., Ueki, K., Sugiura, S., et al. (2009). CD8+ effector T cells contribute to macrophage recruitment and adipose tissue inflammation in obesity. *Nat. Med.* 15, 914–920.
- Orlova, V.V., van den Hil, F.E., Petrus-Reurer, S., Drabsch, Y., Ten Dijke, P., and Mummery, C.L. (2014). Generation, expansion and functional analysis of endothelial cells and pericytes derived from human pluripotent stem cells. *Nat. Protoc.* 9, 1514–1531.
- Patsch, C., Challet-Meylan, L., Thoma, E.C., Ulrich, E., Heckel, T., O'Sullivan, J.F., Grainger, S.J., Kapp, F.G., Sun, L., Christensen, K., et al. (2015). Generation of vascular endothelial and smooth muscle cells from human pluripotent stem cells. *Nat. Cell Biol.* 17, 994–1003.
- Qin, S.X., Cobbold, S., Benjamin, R., and Waldmann, H. (1989). Induction of classical transplantation tolerance in the adult. *J. Exp. Med.* 169, 779–794.
- Qin, S.X., Wise, M., Cobbold, S.P., Leong, L., Kong, Y.C., Parnes, J.R., and Waldmann, H. (1990). Induction of tolerance in peripheral T cells with monoclonal antibodies. *Eur. J. Immunol.* 20, 2737–2745.
- Raval, Z., and Losordo, D.W. (2013). Cell therapy of peripheral arterial disease: from experimental findings to clinical trials. *Circ. Res.* 112, 1288–1302.
- Setiady, Y.Y., Coccia, J.A., and Park, P.U. (2010). In vivo depletion of CD4+FOXP3+ Treg cells by the PC61 anti-CD25 monoclonal antibody is mediated by FcγRIIIb+ phagocytes. *Eur. J. Immunol.* 40, 780–786.
- Simons, M. (2005). Angiogenesis, arteriogenesis, and diabetes: paradigm reassessed? *J. Am. Coll. Cardiol.* 46, 835–837.
- Stabile, E., Burnett, M.S., Watkins, C., Kinnaird, T., Bachis, A., la Sala, A., Miller, J.M., Shou, M., Epstein, S.E., and Fuchs, S. (2003). Impaired arteriogenic response to acute hindlimb ischemia in CD4-knockout mice. *Circulation* 108, 205–210.
- Steinberger, J., and Daniels, S.R. American Heart Association Atherosclerosis, Hypertension, and Obesity in the Young Committee (Council on Cardiovascular Disease in the Young); American Heart Association Diabetes Committee (Council on Nutrition, Physical Activity, and Metabolism) (2003). Obesity, insulin resistance, diabetes, and cardiovascular risk in children: an American Heart Association scientific statement from the Atherosclerosis, Hypertension, and Obesity in the Young Committee (Council on Cardiovascular Disease in the Young) and the Diabetes Committee (Council on Nutrition, Physical Activity, and Metabolism). *Circulation* 107, 1448–1453.
- Tempel, D., de Boer, M., van Deel, E.D., Haasdijk, R.A., Duncker, D.J., Cheng, C., Schulte-Merker, S., and Duckers, H.J. (2012). Apelin enhances cardiac neovascularization after myocardial infarction by recruiting aplnr+ circulating cells. *Circ. Res.* 111, 585–598.
- Tian, X.Y., Wong, W.T., Wang, N., Lu, Y., Cheang, W.S., Liu, J., Liu, L., Liu, Y., Lee, S.S., Chen, Z.Y., et al. (2012a). PPAR α activation protects endothelial function in diabetic mice. *Diabetes* 61, 3285–3293.
- Tian, X.Y., Wong, W.T., Xu, A., Lu, Y., Zhang, Y., Wang, L., Cheang, W.S., Wang, Y., Yao, X., and Huang, Y. (2012b). Uncoupling protein-2 protects endothelial function in diet-induced obese mice. *Circ. Res.* 110, 1211–1216.
- Tsui, N.B., Jiang, P., Wong, Y.F., Leung, T.Y., Chan, K.C., Chiu, R.W., Sun, H., and Lo, Y.M. (2014). Maternal plasma RNA sequencing for genome-wide transcriptomic profiling and identification of pregnancy-associated transcripts. *Clin. Chem.* 60, 954–962.
- van Weel, V., Toes, R.E., Seghers, L., Deckers, M.M., de Vries, M.R., Eilers, P.H., Sipkens, J., Schepers, A., Eefting, D., van Hinsbergh, V.W., et al.

(2007). Natural killer cells and CD4⁺ T-cells modulate collateral artery development. *Arterioscler. Thromb. Vasc. Biol.* 27, 2310–2318.

Weirather, J., Hofmann, U.D., Beyersdorf, N., Ramos, G.C., Vogel, B., Frey, A., Ertl, G., Kerkau, T., and Frantz, S. (2014). Foxp3⁺ CD4⁺ T cells improve healing after myocardial infarction by modulating monocyte/macrophage differentiation. *Circ. Res.* 115, 55–67.

Winer, S., Chan, Y., Paltser, G., Truong, D., Tsui, H., Bahrami, J., Dorfman, R., Wang, Y., Zielenski, J., Mastronardi, F., et al. (2009). Normalization of

obesity-associated insulin resistance through immunotherapy. *Nat. Med.* 15, 921–929.

Wynn, T.A., and Vannella, K.M. (2016). Macrophages in tissue repair, regeneration, and fibrosis. *Immunity* 44, 450–462.

Zhou, L., Sun, K., Zhao, Y., Zhang, S., Wang, X., Li, Y., Lu, L., Chen, X., Chen, F., Bao, X., et al. (2015). Linc-YY1 promotes myogenic differentiation and muscle regeneration through an interaction with the transcription factor YY1. *Nat. Commun.* 6, 10026.

Cell Reports, Volume 24

Supplemental Information

Regulatory T Cells Promote

Apelin-Mediated Sprouting

Angiogenesis in Type 2 Diabetes

Oscar M. Leung, Jiatao Li, Xisheng Li, Vicken W. Chan, Kevin Y. Yang, Manching Ku, Lu Ji, Hao Sun, Herman Waldmann, Xiao Yu Tian, Yu Huang, James Lau, Bin Zhou, and Kathy O. Lui

Supplemental Figures

Figure S1 EC density and tissue infiltrating CD4⁺ T-cells are negatively correlated in T2D patients with PAD, Related to Figure 1. Flow cytometric analysis of (A) %CD31⁺CD144⁺ or (B) %CD4⁺CD3⁺ cells in ischemic muscles of normoglycemic (n=5) and T2D (n=8) patients with PAD, respectively.

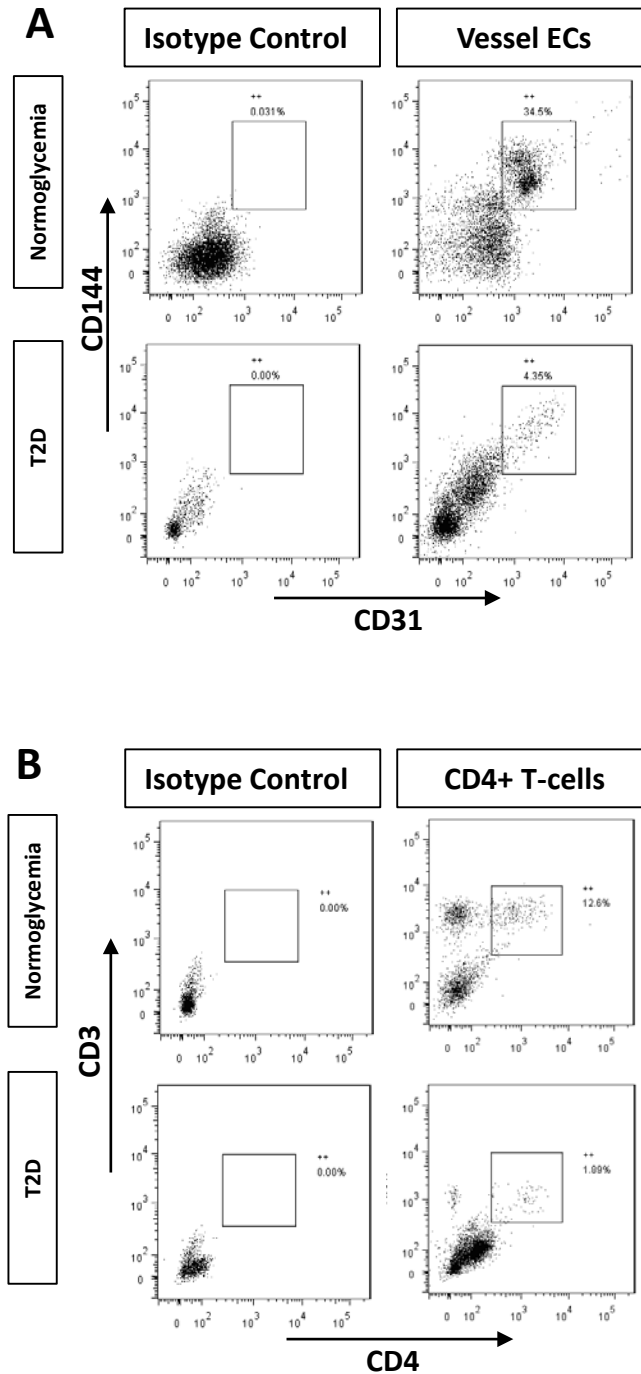
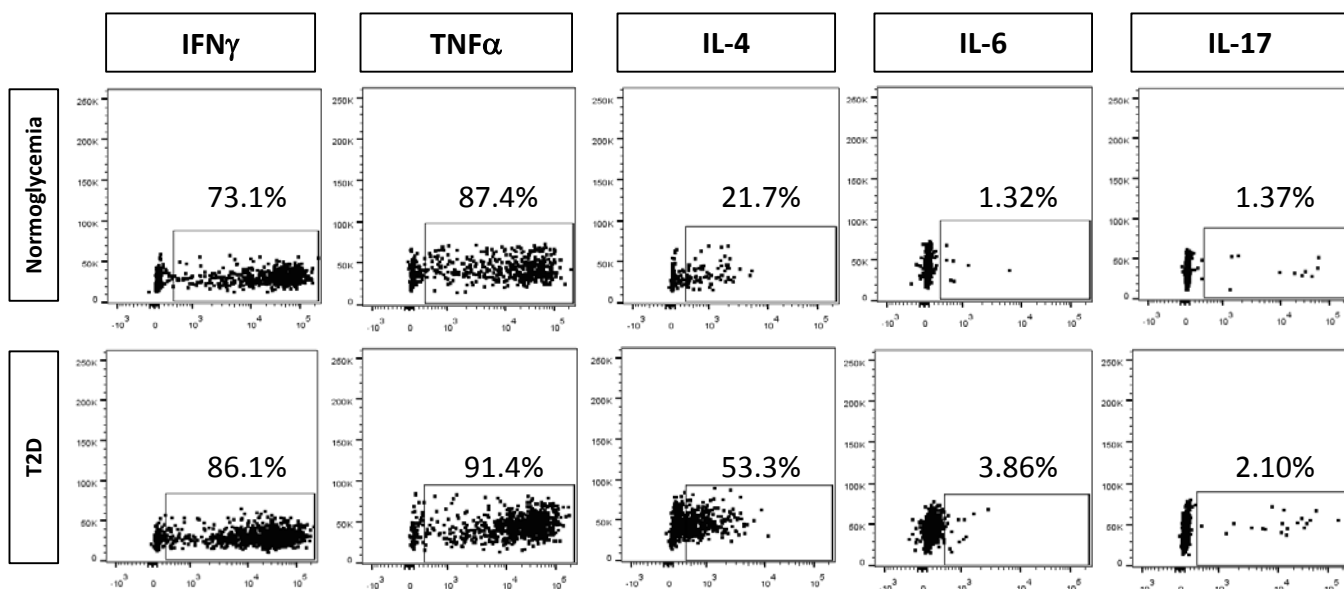
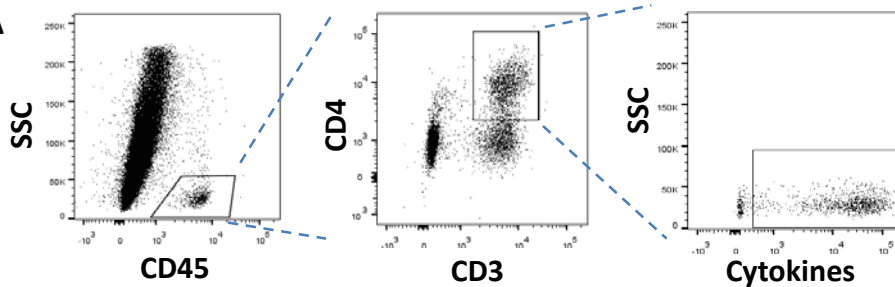


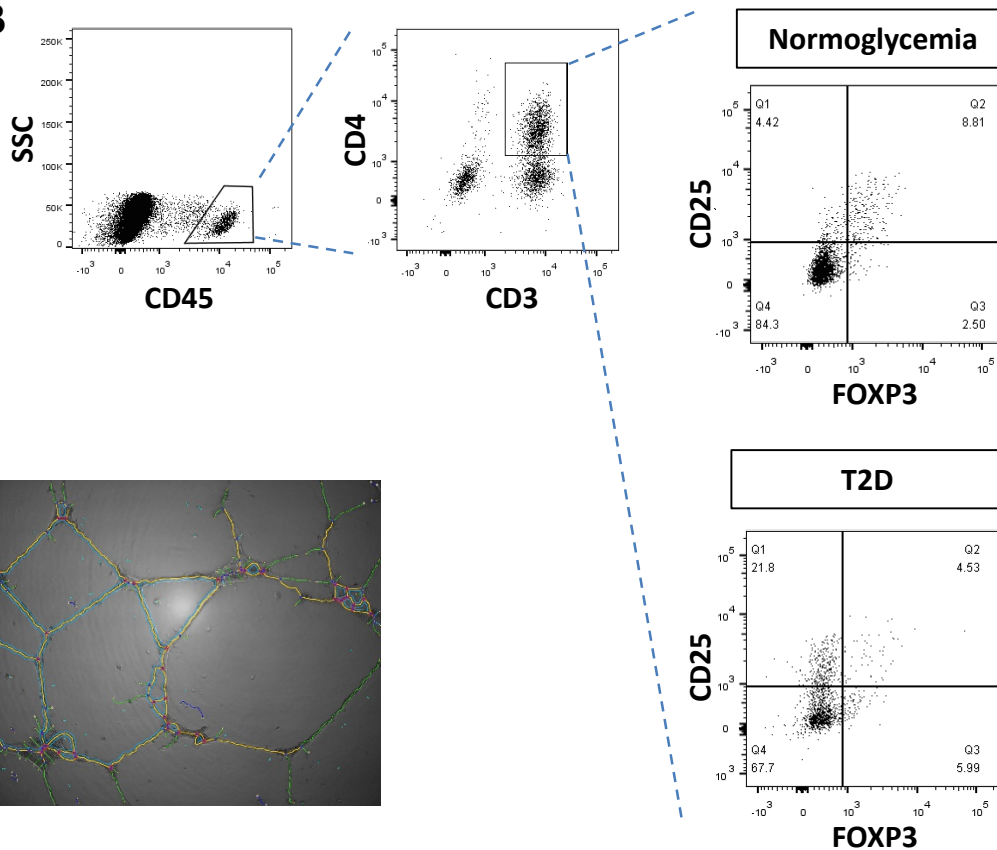
Figure S2 Strategy for analyzing human CD4⁺ T-cell subsets and quantifying *in vitro* human angiogenesis assay, Related to Figure 1. (A) Gating strategy of flow cytometry showing intracellular cytokine-expressing cells demonstrated by first gating on CD45⁺ cells and then on CD3⁺CD4⁺ cells. Absolute cell numbers of IFN γ , TNF α , IL-4, IL-6 or IL-17-expressing cells isolated from ischemic muscles of normoglycemic (n=3) or T2D (n=4) patients with PAD were then quantified, respectively. (B) Gating strategy of flow cytometry showing CD25⁺FOXP3⁺ Treg cells demonstrated by first gating on CD45⁺ cells and then on CD3⁺CD4⁺ cells. Absolute cell numbers of CD4⁺CD25⁺FOXP3⁺ cells isolated from ischemic muscles of normoglycemic (n=3) or T2D (n=4) patients with PAD were then quantified, respectively. (C) ImageJ analysis showing quantification of tube networks and analysis of total tubule length by the Angiogenesis Analyzer plugin.

Fig S2

A



B



C

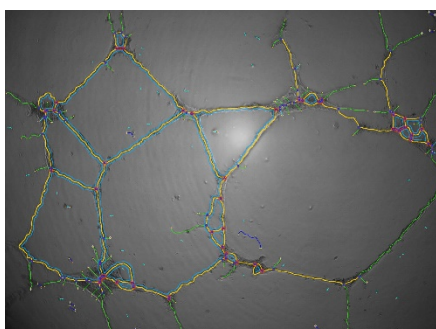


Figure S3 EC density and tissue infiltrating CD4⁺ T-cells are negatively correlated in T2D mice after ischemia, Related to Figure 2. (A) Gating strategy of flow cytometry showing ECs were analyzed by gating on CD45⁻ cells and CD4⁺ T-cells were analyzed by gating on CD45⁺ cells. Flow cytometric analysis of (B) CD45⁻CD31⁺ or (C) CD4⁺CD3⁺ cells in ischemic and non-ischemic muscles of Lepr^{db/+} (n=20) or Lepr^{db/db} (n=20) mice, respectively. Absolute cell numbers of each population were then quantified with these gating strategies.

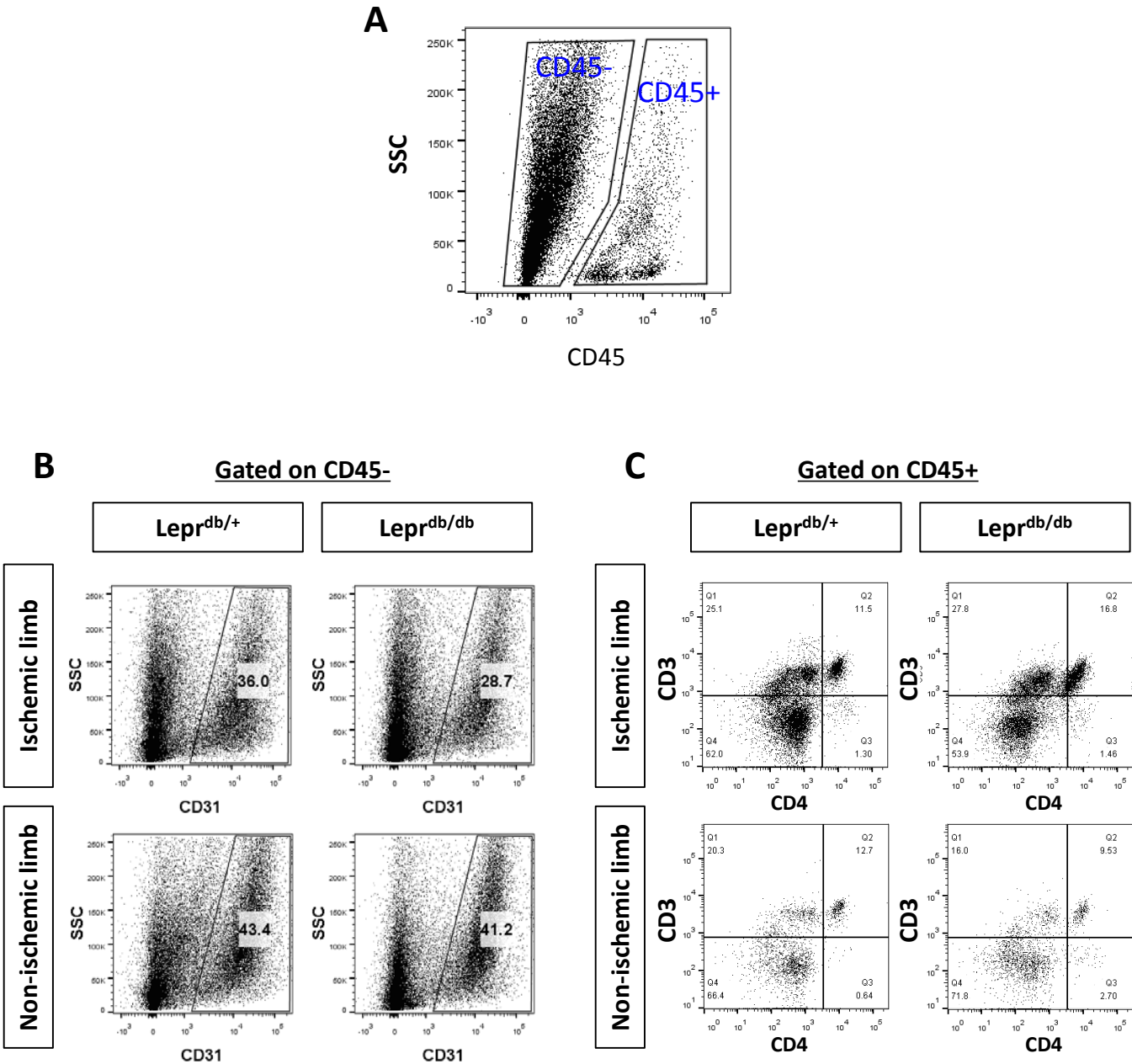


Figure S4 $Lepr^{db/db}$ display impaired vascular function than $Lepr^{db/+}$ mice, Related to Figure 2. (A) Laser Doppler images and (B) quantifications of ischemic/non-ischemic limb perfusion index showing a time-dependent dynamic change in blood flow of $Lepr^{db/db}$ compared to $Lepr^{db/+}$ mice. Data are presented as mean \pm SD, n=10 per group. *indicates $p<0.05$ and ** $p<0.01$.

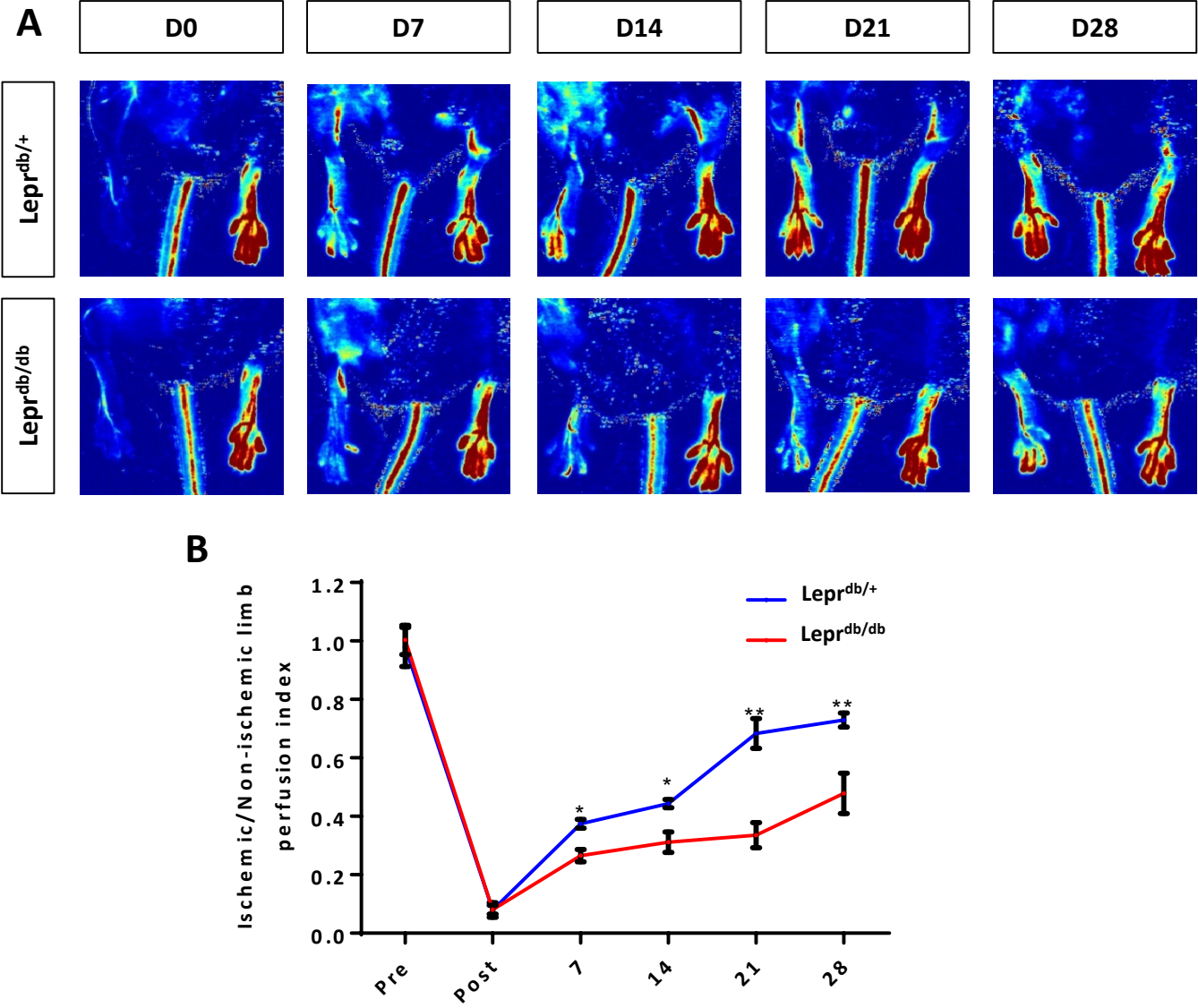


Figure S5 EC density and tissue infiltrating CD4⁺ T-cells are negatively correlated in YTS177-treated T2D mice after ischemia, Related to Figure 3. (A) Gating strategy of flow cytometry showing ECs were analyzed by gating on CD45⁻ cells and CD4⁺ T-cells were analyzed by gating on CD45⁺ cells. Flow cytometric analysis of (B) CD45⁻CD31⁺ or (C) CD4⁺CD3⁺ cells in ischemic and non-ischemic muscles of IgG2a- (n=20) or YTS177-treated (n=20) *Lepr^{db/db}* mice, respectively. Absolute cell numbers of each population were then quantified with these gating strategies.

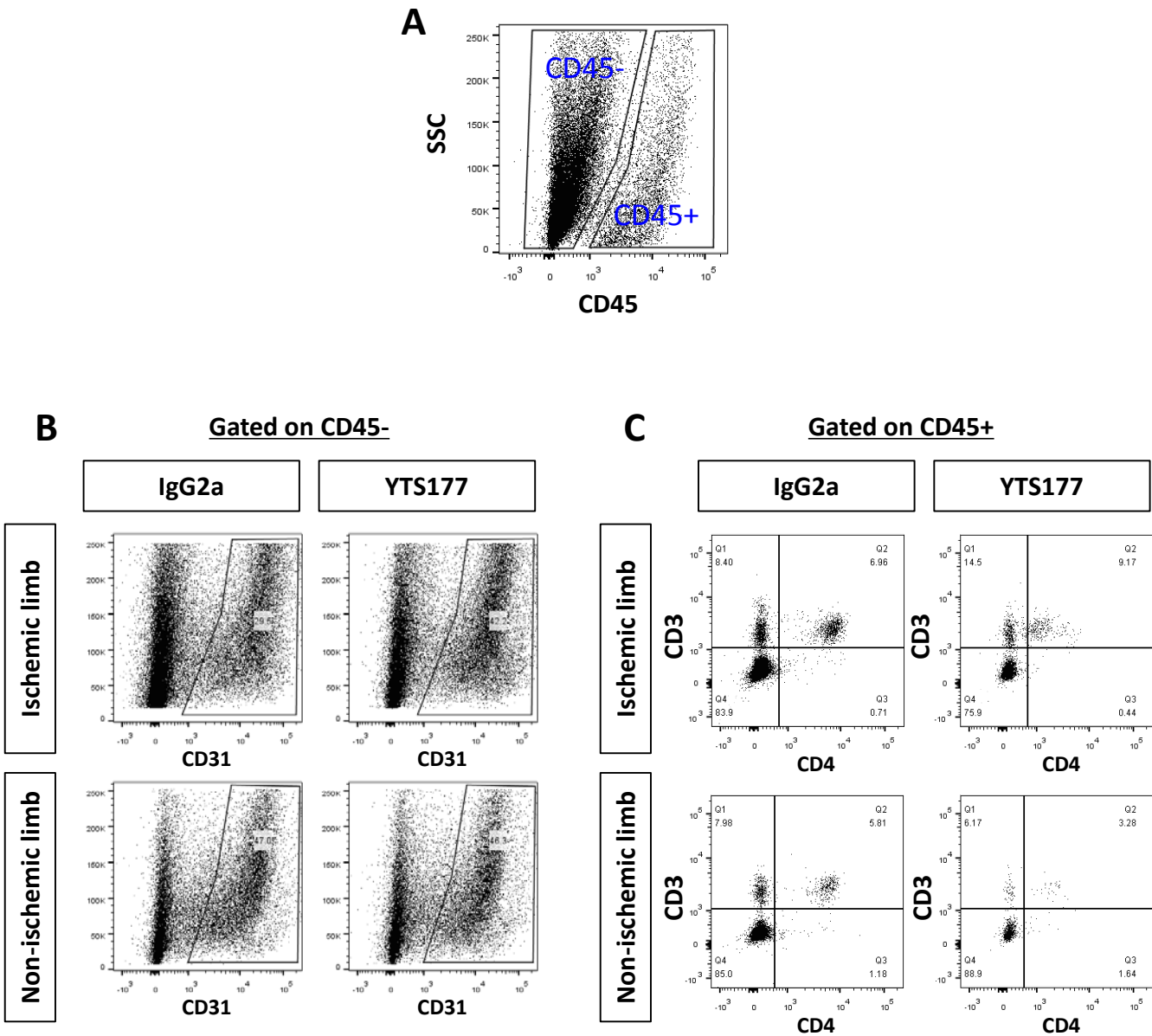


Figure S6 CD4 coreceptor blockade reduces promotes vascular regeneration and reduces vascular inflammation in $Lepr^{db/db}$, Related to Figure 3 (A) Immunostaining and quantification for CD31⁺ cells showing capillary density in ischemic and non-ischemic muscles of IgG2a- (n=6) or YTS177-treated (n=6) $Lepr^{db/db}$, respectively, scale bars: 50 μ m. (B) Quantitative RT-PCR of CD45⁺CD31⁺ ECs purified by flow cytometry from non-ischemic and ischemic muscles of IgG2a- (n=6) or YTS177-treated (n=6) $Lepr^{db/db}$, respectively; expression levels of EC-specific and smooth muscle cell-specific genes were compared to that of control muscle cells. (C) Quantitative RT-PCR of CD45⁺CD31⁺ ECs purified by flow cytometry from ischemic muscles of IgG2a- (n=6) or YTS177-treated (n=6) $Lepr^{db/db}$, respectively; expression levels of pro-inflammatory cytokine genes in the YTS177 group were compared to that of IgG2a. (B, C) All data are presented as mean \pm S.E.M. *indicates $p < 0.05$, ** $p < 0.01$ and *** $p < 0.001$.

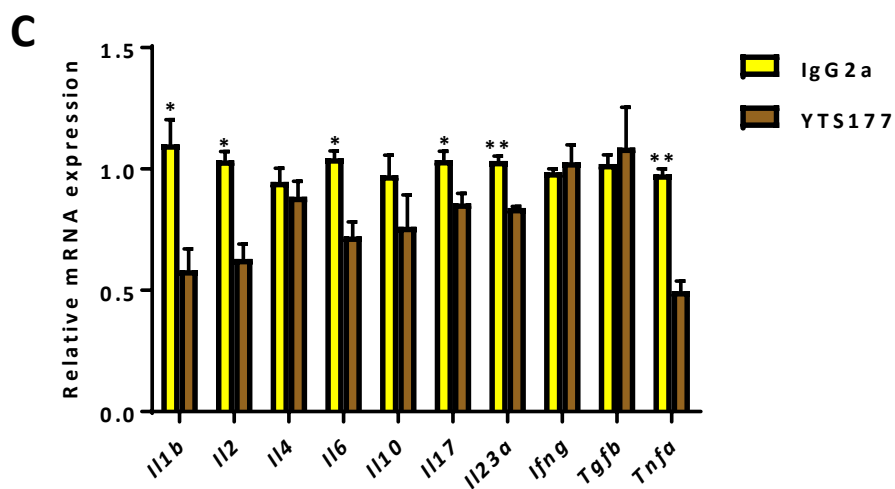
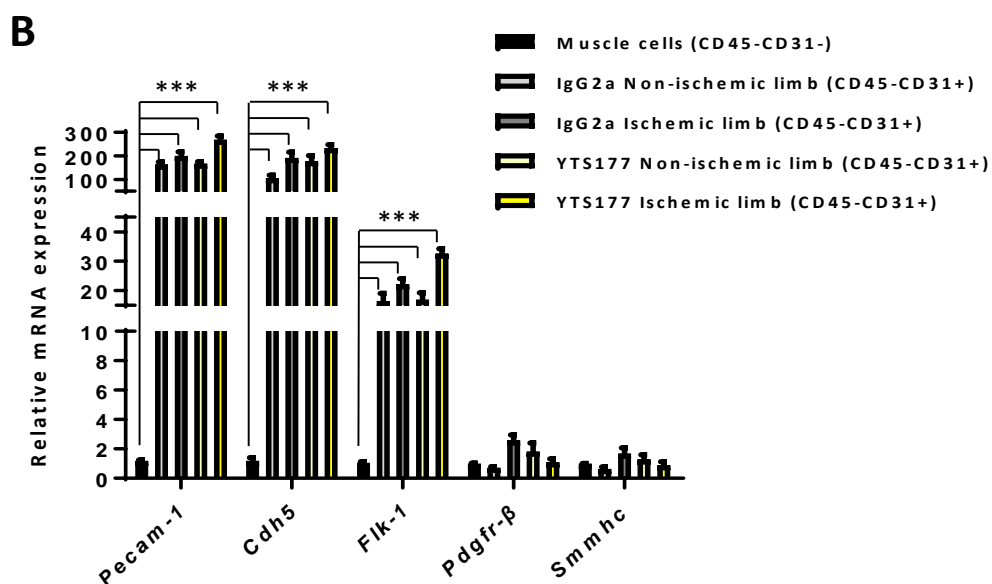
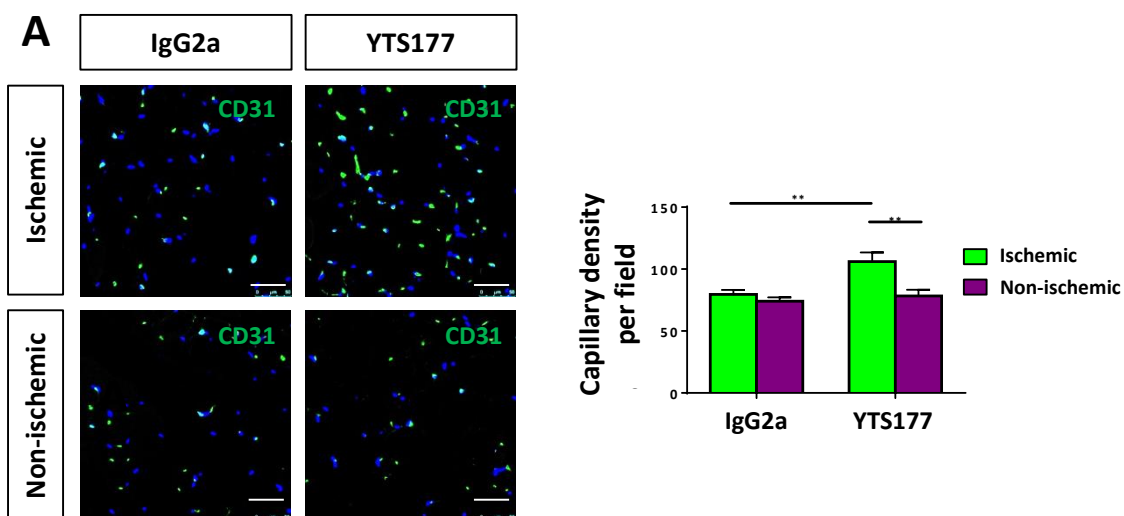
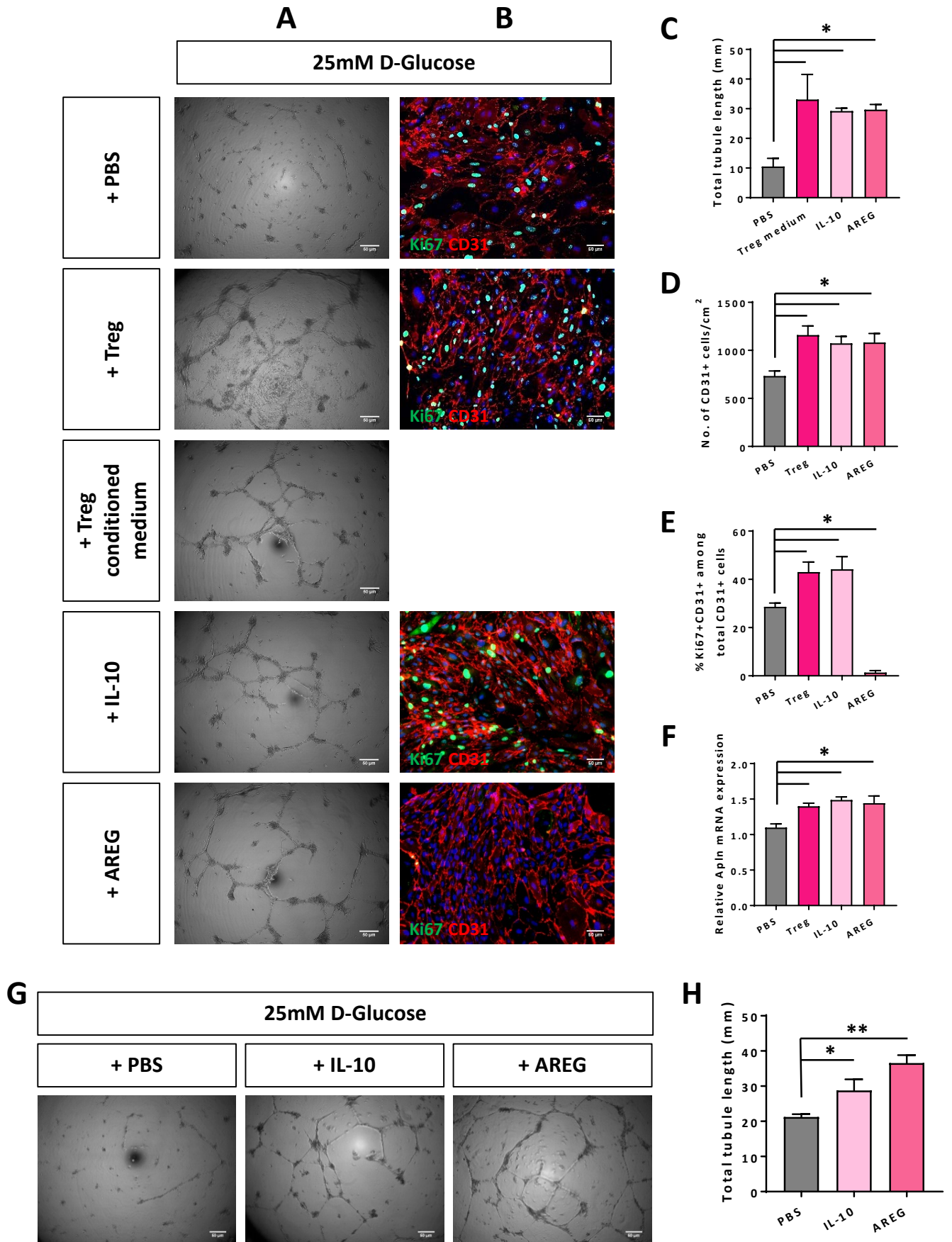


Figure S7 Treg directly promote angiogenesis in hyperglycemia in a paracrine manner, Related to Figure 7. (A) *In vitro* tube formation assay; and (B) immunostaining for Ki67⁺ (green) and CD31⁺ (red) cells with nuclear DAPI counterstain (blue) on primary mouse ECs cultured in high glucose condition (25 mM D-glucose) with PBS (solvent control), Treg, Treg-derived conditioned medium, IL-10 or Amphiregulin (AREG), Quantification of (C) tube formation showing total tubule length, or immunostaining showing (B) total CD31⁺ cells per unit area, or (E) %Ki67⁺CD31⁺ cells among total CD31⁺ cells. (F) Quantitative RT-PCR of ECs from cultures; expression levels of *Apln* by ECs cultured with Treg, IL-10 or AREG were compared to that with PBS. (G) *In vitro* tube formation assay and (H) quantification of total tubule length of hESC-ECs cultured in 25 mM D-glucose with PBS, IL-10 or AREG. Scale bars: (A) 50 μ m, (B) 40 μ m, (G) 50 μ m. (C-F, H) All data are presented as mean \pm S.E.M. *indicates $p < 0.05$ and ** $p < 0.01$.

Fig S7



Supplemental Tables

Table S1 Background information of patients with peripheral artery disease (PAD) included in this study, Related to Figure 1

| PAD Group | Age | Sex | HbA1c level before amputation | Medication for blood glucose control |
|------------------|------------|------------|--------------------------------------|---|
| Normoglycemia | 65 | M | n/a | n/a |
| | 73 | F | n/a | n/a |
| | 80 | F | n/a | n/a |
| | 68 | M | n/a | n/a |
| | 82 | F | n/a | n/a |
| | 59 | M | n/a | n/a |
| | 79 | M | n/a | n/a |
| | 77 | F | n/a | n/a |
| | | | | |
| T2D | 78 | F | 7.4 | Metformin |
| | 52 | F | 13.2 | Metformin |
| | 81 | M | 12.2 | Insulin |
| | 59 | M | 7.6 | Metformin |
| | 83 | F | 12.5 | Metformin, Diamicon |
| | 87 | F | 8.4 | Metformin |
| | 82 | F | 7.9 | Metformin |
| | 83 | F | 9.7 | Declined treatment |
| | 51 | M | 7.1 | Metformin |
| | 79 | F | 7.2 | Metformin, Insulin |
| | 64 | F | 8.7 | Metformin, Insulin |
| | 60 | M | 14.7 | Metformin, Insulin |

Table S2 GO enrichment analyses showing a list of genes expressed by ECs of *Lepr^{db/db}* compared to that of *Lepr^{db/+}* mice within the top 15 pathways in terms of biological processes that were most significantly upregulated as determined by genome-wide transcriptome profiling, Related to Figure 2

| Pathway | p-value | Molecules |
|---|----------------|--|
| GO:0006955~ Immune response | 4.11E-04 | ORAI1, CXCL3, RELB, IL1RN, CCL9, TNFSF13, FCGR1, CCL4, C1QC, CFP, OSM, RAET1C, C1QB, SLC11A1, RAET1D, SERPINA3G, CD300A, IRF7, FCER1G, H2-T22, AF251705, LBP, CLEC5A, CD14 |
| GO:0006954~ Inflammatory response | 9.73E-04 | CXCL3, SPHK1, SAA3, MECOM, C1QC, CCL4, CHST1, CFP, C1QB, SLC11A1, NLR4, PYCARD, LBP, CD14 |
| GO:0001819~ Positive regulation of cytokine production | 0.001888 | RAET1C, SLC11A1, RAET1D, PYCARD, FCER1G, CD40, LBP, CD14 |
| GO:0001817~ Regulation of cytokine production | 0.0027 | RAET1C, SLC11A1, RAET1D, CEBPB, SPHK1, PYCARD, FCER1G, CD40, LBP, CD14, SCAMP5 |
| GO:0009611~ Response to wounding | 0.00283 | CXCL3, SPHK1, SAA3, MECOM, C1QC, CCL4, PLAUR, CHST1, CFP, C1QB, SLC11A1, ARG1, NLR4, GP1BB, PYCARD, LBP, CD14 |
| GO:0050778~ Positive regulation of immune response | 0.008085 | CFP, RAET1C, C1QB, SLC11A1, RAET1D, HPX, FCER1G, TNFSF13, LBP, C1QC |
| GO:0002250~ Adaptive immune response | 0.008513 | C1QB, SLC11A1, IRF7, RELB, FCER1G, TNFSF13, C1QC |
| GO:0002684~ Positive regulation of immune system process | 0.011994 | CFP, RAET1C, C1QB, SLC11A1, RAET1D, HPX, FCER1G, TNFSF13, CD40, LBP, BAD, C1QC |
| GO:0002252~ Immune effector process | 0.017182 | CFP, C1QB, SLC11A1, IRF7, FCER1G, TNFSF13, LBP, C1QC |
| GO:0002449~ Lymphocyte mediated immunity | 0.02191 | C1QB, SLC11A1, IRF7, FCER1G, TNFSF13, C1QC |
| GO:0002712~ Regulation of B cell mediated immunity | 0.024634 | HPX, FCER1G, TNFSF13, CD40 |
| GO:0006917~ Induction of apoptosis | 0.025073 | PLEKHF1, CEBPB, BNIP1, BOK, APOE, PYCARD, NDUFA13, NGFRAP1, BAD |
| GO:0012502~ Induction of programmed cell death | 0.025073 | PLEKHF1, CEBPB, BNIP1, BOK, APOE, PYCARD, NDUFA13, NGFRAP1, BAD |
| GO:0002822~ Regulation of adaptive immune response based on somatic recombination of immune receptors built from immunoglobulin superfamily domains | 0.030019 | SLC11A1, HPX, FCER1G, TNFSF13, CD40 |
| GO:0002819~ Regulation of adaptive immune response | 0.030019 | SLC11A1, HPX, FCER1G, TNFSF13, CD40 |

Table S3 GO enrichment analyses showing a list of genes expressed by ECs of Lepr^{db/db} mice treated with YTS177 compared to that of IgG2a within the top 10 pathways in terms of biological processes that were most significantly upregulated as determined by genome-wide transcriptome profiling, Related to Figure 3

| Pathway | p-value | Molecules |
|--|----------------|--|
| GO:0051301~Cell division | 4.27E-06 | BMI1, SEPT2, PRC1, SYCE2, ANAPC10, LIG4, CDC25C, UBE2C, FAM83D, CCNB1, DCLRE1A, MAD2L1, CCNB2, NCAPG2, CDC123, ARL8B, CCNA2, STAG2, CDCA3, ZW10 |
| GO:0007067~Mitosis | 3.12E-05 | SEPT2, ANAPC10, CDC25C, UBE2C, CCNB1, FAM83D, DCLRE1A, CCNB2, MAD2L1, NCAPG2, ARL8B, CCNA2, STAG2, CDCA3, ZW10 |
| GO:0000280~Nuclear division | 3.12E-05 | SEPT2, ANAPC10, CDC25C, UBE2C, CCNB1, FAM83D, DCLRE1A, CCNB2, MAD2L1, NCAPG2, ARL8B, CCNA2, STAG2, CDCA3, ZW10 |
| GO:0000278~Mitotic cell cycle | 3.61E-05 | SEPT2, ANAPC10, CDC25C, UBE2C, FAM83D, CCNB1, DCLRE1A, MAD2L1, CCNB2, NCAPG2, CDC123, STMN1, ARL8B, CCNA2, STAG2, CDCA3, ZW10 |
| GO:0000087~M phase of mitotic cell cycle | 3.93E-05 | SEPT2, ANAPC10, CDC25C, UBE2C, CCNB1, FAM83D, DCLRE1A, CCNB2, MAD2L1, NCAPG2, ARL8B, CCNA2, STAG2, CDCA3, ZW10 |
| GO:0048285~Organelle fission | 4.66E-05 | SEPT2, ANAPC10, CDC25C, UBE2C, CCNB1, FAM83D, DCLRE1A, CCNB2, MAD2L1, NCAPG2, ARL8B, CCNA2, STAG2, CDCA3, ZW10 |
| GO:0000279~M phase | 6.24E-05 | NBN, SEPT2, SYCE2, ANAPC10, CDC25C, UBE2C, FAM83D, CCNB1, DCLRE1A, MAD2L1, CCNB2, NCAPG2, STMN1, ARL8B, CCNA2, STAG2, CDCA3, ZW10 |
| GO:0007155~Cell adhesion | 7.00E-05 | PCDHA9, PCDHA2, PCDHA4, NPNT, TNC, POSTN, DDR2, PCDHAC1, GLYCAM1, COL6A1, COL12A1, CD4, DPT, THBS4, PTPRC, SELL, ITGA1, CPXM2, NID1, KITL, COL5A1, CD84, DDR1, SIGLEC1, COL14A1, CPXM1, NPTN, ANTXR1, PERP, ADAM12 |
| GO:0000279~Cell cycle phase | 1.22E-04 | NBN, SEPT2, SYCE2, ANAPC10, CDC25C, UBE2C, FAM83D, CCNB1, DCLRE1A, CCNB2, MAD2L1, NCAPG2, CDC123, STMN1, ARL8B, CCNA2, STAG2, CDCA3, ZW10 |
| GO:0022402~Cell cycle process | 0.001048 | NBN, SEPT2, SYCE2, ANAPC10, CDC25C, UBE2C, FAM83D, CCNB1, DCLRE1A, CCNB2, MAD2L1, NCAPG2, CDC123, STMN1, ARL8B, CCNA2, STAG2, CDCA3, ZW10 |